CMS Physics Analysis Summary

Contact: cms-pag-conveners-susy@cern.ch 2015/10/31

Phenomenological MSSM interpretation of CMS results at $\sqrt{s} = 7$ and 8 TeV

The CMS Collaboration

Abstract

Using a global Bayesian analysis, it is shown how the results from searches for supersymmetry performed by CMS constrain the Minimal Supersymmetric Standard Model (MSSM). The study is performed within the framework of the phenomenological MSSM (pMSSM), a 19-parameter realization of the R-parity conserving weak-scale MSSM, that captures most of the latter's phenomenological features and which, therefore, permits robust conclusions to be drawn about the MSSM. It is found that all pMSSM points considered with a gluino mass below 500 GeV are excluded. In the mass range between 500 GeV and 1400 GeV, there are many scenarios that cannot as yet be excluded, contrary to current gluino mass limits using simplified models. Similar conclusions are made for squarks, charginos, and neutralinos. The mass of the lighter top squark $\tilde{t}_1$ is found to be unconstrained and, therefore, a relatively light $\tilde{t}_1$ cannot be excluded in the pMSSM context. Constraints on the pMSSM parameter space provided by the Higgs boson signal strength measurements do not alter the conclusions drawn from the direct searches for supersymmetry. The results used in this analysis are based on datasets from proton-proton collisions at 7 TeV and 8 TeV with integrated luminosities of 5.0 fb^{-1} and 19.5 fb^{-1}, respectively.

1 Introduction

As of this date, discovery [1, 2] of a Higgs boson is clearly the most significant observation from the Large Hadron Collider (LHC). Almost as significant, however, is the absence of any compelling sign of new physics. In particular, there is no hint of supersymmetry (SUSY) (see Refs. [3, 4] for an introduction to SUSY).

If SUSY does not manifest in experiments at the TeV scale, large changes in focus will likely take place within the particle physics community. However, the absence of evidence should not yet be taken as evidence of absence. Searches for SUSY have been interpreted within constrained models with just a few parameters, such as the Constrained Minimal Supersymmetric Standard Model (CMSSM) [5–11], or more recently within the Simplified Model Spectra (SMS) approach [12–14]. However, the full diversity of mass spectra and event signatures of supersymmetry, in particular, of the Minimal Supersymmetric Standard Model (MSSM), is not necessarily realized in these approaches. Constrained models feature specific relations between the soft-breaking terms at some mediation scale, which translate into specific mass patterns typical for the model. While this problem is avoided in the SMS approach, the signatures of realistic models cannot always be fully covered by SMS topologies. This holds true, for instance, in the case of long decay chains that do not correspond to any SMS, t-channel exchanges of virtual sparticles in production, or other decay processes that change the kinematic distributions. Finally, the limit from several search channels taken together may exclude certain parameter regions, while they would be allowed when considering each analysis separately. Sensitivity can increase substantially in the case of a large diversity of decay modes that give rise to a mix of signatures.

It is therefore interesting and timely to investigate how a variety of CMS SUSY searches taken together in a global approach currently constrain the MSSM. This is the goal of this paper. Specifically, we interpret the CMS results in terms of the phenomenological MSSM (pMSSM) [15], a 19-dimensional realization of the R-parity conserving weak-scale MSSM that captures most of the latter's phenomenological features. Here, R-parity is a $\mathbb{Z}_2$ symmetry forbidding the violation of lepton and baryon number. In the pMSSM, all MSSM parameters are specified at the electroweak scale and allowed to vary freely subject to the requirement that the model be consistent with electroweak symmetry breaking (EWSB) and other such basic constraints. Since the pMSSM includes neither relations between SUSY breaking terms at a high scale, nor large correlations between sparticle masses from renormalization group evolution, it allows a much broader set of scenarios than those in, for example, the CMSSM and related GUT-scale models. Many of these scenarios are difficult to constrain using current LHC data — in particular, scenarios with low SUSY masses can evade detection.

In order to assess what the data obtained by CMS do and do not tell us about SUSY in the context of the pMSSM, we use a representative subset of the results obtained by CMS based on datasets corresponding to integrated luminosities of 5.0 fb^{-1} at 7 TeV and 19.5 fb^{-1} at 8 TeV. We use results from hadronic searches, both general searches and ones that target stop production, and electroweak (EW) searches with leptonic final states. Because this study uses a fast detector simulation that does not model accurately the detector response to massive long-lived charged particles, we work within a subspace of the pMSSM in which the chargino lifetime $c\tau(\tilde{\chi}_1^{\pm})$ is less than 10 mm, which restricts the class of final states considered to those with prompt decays. The 7 TeV and 8 TeV data are treated identically, in particular, we use the same set of pMSSM model points chosen randomly from a larger set of points that are consistent with pre-LHC experimental results and basic theoretical constraints. This greatly facilitates the combination of the 7 and 8 TeV data.

The approach employed is an extension of the pioneering work of Ref. [16], which interpreted three independent CMS analyses based on $\sim$1 fb^{-1} of CMS data [17–19] in terms of the pMSSM, confirming that the approach is both feasible and better at obtaining general conclusions about SUSY than those based on constrained SUSY models. Furthermore, the diversity of phenomena covered by the pMSSM is also helpful in suggesting new approaches to searches for SUSY at the LHC. This study follows closely the Bayesian approach [20, 21] used in Ref. [16].

The paper is organized as follows. The definition of the pMSSM is given in Section 2. Section 3 describes our analysis, which includes the construction of a prior for the pMSSM model and the calculation of likelihoods for the CMS results. The results of this study are presented in Section 4, including discussions of the impact of the CMS searches and their current sensitivity to the pMSSM. Section 6 contains our conclusions.

2 Definition of the phenomenological MSSM

A priori, the weak-scale MSSM has 120 free parameters, assuming that R-parity is conserved (to avoid proton decay and to ensure that the lightest SUSY particle, the LSP, is stable) and assuming that the gravitino is heavy. This is clearly too large a parameter space for any phenomenological study. However, most of these parameters are associated with CP-violating phases and, or, flavor changing neutral currents (FCNC), which are severely constrained by experiment. Therefore, a few reasonable assumptions about the flavor and CP structure allow a reduction in the number of free parameters by a factor six, without imposing any SUSY breaking mechanism. This has the virtue of avoiding relations, which need not hold in general, between the soft terms introduced by models of SUSY breaking.

Strong constraints on CP violation are satisfied by taking all parameters to be real, and FCNC constraints are satisfied by taking all sfermion mass matrices and trilinear couplings to be flavor-diagonal. Moreover, the first two generations of sfermions are taken to be degenerate. Regarding the trilinear A-terms of the first two generations, these only enter phenomenology multiplied by the associated very small Yukawa couplings and are thus not experimentally relevant. Only the third generation parameters A_t, A_b and A_τ have consequences that are potentially observable.

This leaves 19 real weak-scale SUSY Lagrangian parameters that define the pMSSM [15]. As noted above, the pMSSM captures most of the phenomenological features of the R-parity conserving MSSM and, most importantly, encompasses and goes beyond a broad range of more constrained SUSY models. The free parameters of the pMSSM are:

- three independent gaugino mass parameters M_1, M_2, and M_3,
- the ratio of the Higgs vacuum expectation values $\tan\beta = v_2/v_1$,
- the higgsino mass parameter μ and the pseudo-scalar Higgs boson mass m_A,
- 10 independent sfermion mass parameters $m_{\tilde{F}}$, where $\tilde{F} = \tilde{Q}_1$, $\tilde{U}_1$, $\tilde{D}_1$, $\tilde{L}_1$, $\tilde{E}_1$, $\tilde{Q}_3$, $\tilde{U}_3$, $\tilde{D}_3$, $\tilde{L}_3$, $\tilde{E}_3$ (for the 2nd generation we take $m_{\tilde{Q}_2} = m_{\tilde{Q}_1}$, $m_{\tilde{L}_2} = m_{\tilde{L}_1}$, $m_{\tilde{U}_2} = m_{\tilde{U}_1}$, $m_{\tilde{D}_2} \equiv m_{\tilde{D}_1}$, and $m_{\tilde{E}_2} \equiv m_{\tilde{E}_1}$), and
- the trilinear couplings A_t, A_b and A_τ ,

in addition to the standard model (SM) parameters. To minimize theoretical uncertainties in the Higgs sector, these parameters are conveniently defined at the scale, $M_{\rm SUSY} \equiv \sqrt{m_{\tilde{t}_1} m_{\tilde{t}_2}}$, often also referred to as the electroweak symmetry breaking (EWSB) scale.

The pMSSM parameter space is constrained by a number of theoretical requirements. First,

the sparticle spectrum must be free of tachyons and cannot lead to color or charge breaking minima in the scalar potential. We also require that EWSB be consistent and that the Higgs potential be bounded from below. Finally, in this study, we also require that the LSP be the lightest neutralino, $\tilde{\chi}_1^0$. These requirements yield a model that is an excellent proxy for the full MSSM with a sufficiently small number of parameters such that a complete exploration of it is possible given existing computer resources.

It is of interest to note the generic properties of sparticle mass spectra of the pMSSM. By definition, each first generation sfermion is exactly degenerate in mass with the corresponding second generation sfermion. Other generic properties of pMSSM mass spectra are actually MSSM properties; in the first and second generation, spartners of left handed down-type quarks are strongly mass degenerate with the corresponding up-type squarks. Likewise, first and second generation spartners of left handed charged leptons are strongly degenerate with the corresponding sneutrinos. The nature of the spectrum of neutralinos and charginos depends on the relative magnitudes and separation of the pMSSM parameters M_1, M_2 and μ. If these scales are well separated then the approximate eigenstates will divide into: a single bino-like state with mass of order M_1; a wino-like triplet consisting of two charginos and one neutralino with masses of order M_2, and a higgsino-like quartet of two charginos and two neutralinos with masses of order μ. The LSP will then be primarily composed of the neutral member(s) of the lightest of these three. If the parameters above are not well separated, then the LSP will be a mixture of the neutral states.

3 Analysis

The purpose of this study is to assess what current data tell us and do not tell us about the MSSM using the more tractable pMSSM as a proxy. We use the results from several CMS analyses, which cover a variety of final states, to construct posterior densities of model parameters, masses, and observables. The posterior density of the model parameters, which are denoted by θ, is given by

$$p(\theta|D^{\text{CMS}}) \propto L(D^{\text{CMS}}|\theta)\, p^{\text{non-DCS}}(\theta), \tag{1}$$

where D^{CMS} denotes the CMS data, $L(D^{\text{CMS}}|\theta)$ the associated CMS likelihood, and $p^{\text{non-DCS}}(\theta)$ the prior density constructed from results other than those from direct CMS searches (DCS). The posterior density for an observable λ is obtained as follows,

$$p(\lambda|D^{\text{CMS}}) = \int \delta[\lambda - \lambda'(\theta)]\, p(\theta|D^{\text{CMS}})\, d\theta, \tag{2}$$

which is approximated using Monte Carlo integration. In this section, we describe the construction of the prior and CMS likelihoods.

3.1 Construction of the prior

If the posterior density for a given parameter differs significantly from its prior density, then we may conclude that the data have provided useful information about the parameter, otherwise, the converse is true. However, for such conclusions to be meaningful, it is necessary to start with a prior that encodes as much relevant information as possible. When such a prior is combined with a likelihood incorporating a broad set of results, the conclusions arrived at will be globally valid. In this study, the prior density $p^{\text{non-DCS}}(\theta)$ (or prior, for short) encodes several constraints: the parameter space boundary, some theoretical conditions, the chargino lifetimes, and most importantly those from non-direct CMS search (non-DCS) data such as precision measurements or pre-LHC new physics searches.

The prior, $p^{\text{non-DCS}}(\theta)$, is factorized into four terms,

$$p^{\text{non-DCS}}(\theta) \propto \left[\prod_j L(D_j^{\text{non-DCS}}|\mu_j(\theta))\right] p(c\tau(\tilde{\chi}^{\pm}) < 10\,\text{mm}|\theta)\, p(\text{theory}|\theta)\, p_0(\theta). \tag{3}$$

The term $p_0(\theta)$, the *ur-prior* (coined by Glen Cowan from the German prefix *ur* meaning original or primitive), is taken to be flat in the pMSSM sub-space,

$$\begin{gathered} -3\,\text{TeV} \leq M_1, M_2 \leq 3\,\text{TeV} \\ 0 \leq M_3 \leq 3\,\text{TeV} \\ -3\,\text{TeV} \leq \mu \leq 3\,\text{TeV} \\ 0 \leq m_A \leq 3\,\text{TeV} \\ 2 \leq \tan\beta \leq 60 \\ 0 \leq \tilde{Q}_{1,2}, \tilde{U}_{1,2}, \tilde{D}_{1,2}, \tilde{L}_{1,2}, \tilde{E}_{1,2}, \tilde{Q}_3, \tilde{U}_3, \tilde{D}_3, \tilde{L}_3, \tilde{E}_3 \leq 3\,\text{TeV} \\ -7\,\text{TeV} \leq A_t, A_b, A_\tau \leq 7\,\text{TeV}, \end{gathered} \tag{4}$$

and the unbounded SM sub-space defined by m_t, $m_b(m_b)$, and $\alpha_s(M_Z)$. A point in this sub-space is denoted by θ. The sub-space defined in Eq. (4) covers the phenomenologically viable parameter space for the LHC and is large enough to cover sparticle masses to which the LHC might conceivably be ultimately sensitive. The lower bound of 2 for $\tan\beta$ evades non-perturbative effects in the top-quark Yukawa coupling after evolution up to the GUT scale [22]. These effects typically become a very serious issue for $\tan\beta \lesssim 1.7$. The term $p(\text{theory}|\theta)$ imposes the theoretical constraints listed at the end of Section 2, while $p(c\tau(\tilde{\chi}^{\pm}) < 10\,\text{mm}|\theta)$ imposes the prompt chargino constraint. Both $p(\text{theory}|\theta)$ and $p(c\tau(\tilde{\chi}^{\pm}) < 10\,\text{mm}|\theta)$ are unity if the constraints are satisfied and zero otherwise.

The product of likelihoods $L(D^{\text{non-DCS}}|\lambda(\theta))$ in Eq. (3) is associated with non-DCS data ($D^{\text{non-DCS}}$) which imposes constraints from precision measurements and pre-LHC searches for new physics. The data and their associated likelihoods are listed in Table 1. We choose to avoid cosmological assumptions as they contain large uncertainties, and therefore do not include data from dark matter experiments.

Since the explicit functional dependence of the prior $p^{\text{non-DCS}}(\theta)$ on θ is not available *a priori*, but the predictions $\lambda(\theta)$ are available point by point, it is natural to represent the prior as set of points sampled from it. Owing to the complexity of the parameter space, the sampling is done using a Markov Chain Monte Carlo (MCMC) method [21, 23–26].

The non-DCS data included in the prior are shown in Table 1. All data except the Higgs signal strengths μ_h were used in the MCMC scan. It should be noted that the measurements marked "reweight in the last column were updated during the course of this study. This was taken into account by reweighting each of the 7200 scan points by the likelihood ratio of the new and the old measurement. Table 1 gives the final constraints used in the prior; the original ones used in the MCMC sampling and the reweighting procedure are detailed in Appendix A. The Higgs signal strengths were incorporated into the non-DCS likelihood post-MCMC.

For a given point θ, the predictions $\lambda(\theta)$ — including those needed to calculate the likelihoods $L(D^{\text{non-DCS}}|\lambda(\theta))$ — are obtained as follows. The physical masses and interactions are calculated to state-of-the-art accuracy, using the SUSY spectrum generator `SoftSUSY_3.3.1` [27], with the input parameters θ defined at M_{SUSY}. This calculation includes 1-loop corrections for sparticle masses and mixings, as well as 2-loop corrections for the light Higgs boson mass. Low-energy constraints are calculated with `SuperIso_v3.3` [28], and `micrOMEGAs_2.4.5` [29–31] is used to compute the dark matter relic density $\Omega_{\tilde{\chi}_1^0}h^2$, direct detection cross sections at

LEP, and to check compatibility with various pre-LHC sparticle mass limits. The program `SDECAY1.3` [32] is used to calculate sparticle decay tables and `HDECAY5.11` [33] to calculate Higgs boson decay tables. For evaluating the Higgs boson signal likelihood based on the latest ATLAS [34] and CMS [35] measurements, we use `Lilith1.0.1` [36, 37], following the approach explained in Section 2.3 of Ref. [38]. [1] The uncertainty in the anomalous magnetic moment of the muon includes a component that accounts for theoretical uncertainties in the SUSY calculations.

The large window on the Higgs boson mass of 120–130 GeV accounts for the theoretical uncertainty in the Higgs boson mass calculation in the MSSM. All tools use the SUSY Les Houches Accord [39] for data entry and output. Approximately 20 million points are sampled from $p^{\text{non-DCS}}(\theta)$ using multiple MCMC chains, but omitting the prompt chargino requirement. When that requirement is imposed, the number of sampled points is reduced by 30%. A random subsample of 7200 points is selected for simulation studies.

Table 1: The measurements that are the basis of the non-DCS prior $p^{\text{non-DCS}}(\theta)$ for the pMSSM parameters. See text for details.

i	Observable $\mu_i(\theta)$	Constraint $D_i^{\text{non-DCS}}$	Likelihood function $L(D_i^{\text{non-DCS}}\|\mu_i(\theta))$	comment
1	$BR(b \to s\gamma)$ [40]	$(3.43 \pm 0.21^{\text{stat}} \pm 0.24^{\text{th}} \pm 0.07^{\text{sys}}) \times 10^{-4}$	Gaussian	reweight
2	$BR(B_s \to \mu\mu)$ [41]	$(2.9 \pm 0.7 \pm 0.29^{th}) \times 10^{-9}$	Gaussian	reweight
3	$R(B_u \to \tau\nu)$[40]	1.04 ± 0.34	Gaussian	reweight
4	Δa_μ [42]	$(26.1 \pm 6.3^{\text{exp}} \pm 4.9^{\text{SM}} \pm 10.0^{\text{SUSY}}) \times 10^{-10}$	Gaussian	
5	m_t [43]	$173.20 \pm 0.87^{\text{stat}} \pm 1.3^{\text{sys}}$ GeV	Gaussian	reweight
6	$m_b(m_b)$ [44]	$4.19^{+0.18}_{-0.06}$ GeV	Two-sided Gaussian	
7	$\alpha_s(M_Z)$ [44]	0.1184 ± 0.0007	Gaussian	
8	m_h	LHC: $m_h^{low} = 120$, $m_h^{up} = 130$	1 if $m_h^{low} \le m_h \le m_h^{up}$ 0 if $m_h < m_h^{low}$ or $m_h > m_h^{up}$	reweight
9	μ_h	CMS and ATLAS in LHC RunI, Tevatron	`Lilith1.01` [36, 37]	post-MCMC
10	sparticle masses	LEP [45] (via micrOMEGAs [29–31])	1 if allowed 0 if excluded	

3.2 Construction of the CMS likelihoods

We consider the analyses given in Table 2, which explore final state topologies characterized by the event-level variables: the scalar sum of the transverse momenta of jets (HT); the magnitude of the vector sum of the transverse momenta of jets (MHT); a measure of the transverse mass in events with two invisible particles (MT2); the multiplicity of b-tagged jets, and a range of lepton multiplicities. The searches together comprise hundreds of signal regions and address a large diversity of possible signal topologies.

CMS likelihoods $L(D^{\text{CMS}}|\theta)$ are calculated for each of these analyses (or combinations of analyses), using different forms of likelihood depending on the nature of the results that are available. The first form of likelihood (*counts*) uses observed counts, N, and associated background estimates, $B \pm \delta B$; the second (χ^2) uses profile likelihoods, $T(\mu, \theta)$, where $\mu = \sigma/\sigma^{\text{SUSY}}(\theta)$ is

[1] The experimental results used in `Lilith` are the signal strengths for the $h \to Y$, $Y\gamma\gamma$, WW^*, ZZ^*, $b\bar{b}$, $\tau\tau$, decay modes in terms of the primary Higgs production modes gluon–gluon fusion (ggF), vector boson fusion (VBF), associated production with a W or Z boson (WH and ZH, commonly denoted as VH), and associated production with a top-quark pair (ttH) as published by ATLAS and CMS and the Tevatron experiments. When these signal strengths are given as 2D CL contours in, e.g., the $\lambda_{\text{ggF+ttH}}(Y)$ versus $\mu_{\text{VBF+VH}}(Y)$ plane, the likelihood is reconstructed by fitting a 2D Gaussian to the 68% CL contour provided by the experiments. For each experiment, the likelihood is then given by $-2\log L_Y = \chi^2_Y$ for each decay mode Y, and the combined likelihood is then obtained by summing over all the individual χ^2_Ys. Additional information on signal strengths (and invisible decays) in 1D is included analogously, using the published likelihood function when available or else again the Gaussian approximation. .

Table 2: The CMS analyses considered in this study. Listed are the analyses (Analysis), the center-of-mass energy at which data were collected ($\sqrt{s}$), the associated integrated luminosity (L), the likelihood used (Likelihood), and the reference to the analysis documentation (Ref.).

Analysis	$\sqrt{s}$ [TeV]	L [fb^{-1}]	Likelihood
Hadronic HT + MHT search [46]	7	4.98	counts
Hadronic HT + MET + b-jets search [47]	7	4.98	counts
Leptonic search for EW prod. of $\widetilde{\chi}^0$, $\widetilde{\chi}^{\pm}$, $\tilde{l}$ [48]	7	4.98	counts
Hadronic HT + MHT search [49]	8	19.5	counts
Hadronic MT2 search [50]	8	19.5	counts
Hadronic HT + MET + b-jets search [51]	8	19.4	χ^2
Monojet searches [52, 53]	8	19.7	binary
Hadronic stop search [54]	8	19.4	counts
Opposite sign di-lepton (OS ll) search [55] (count experiment only)	8	19.4	counts
Like-sign di-leptoin (LS ll) search [56] (only channels w/o 3rd lepton veto)	8	19.5	counts
Leptonic search for EW prod. of $\widetilde{\chi}^0$, $\widetilde{\chi}^{\pm}$, $\tilde{l}$ [57] (only ss, 3l, and 4l channels)	8	19.5	counts
Combination of 7 TeV searches	7	-	binary
Combination of 8 TeV searches	8	-	binary
Combination of 7 and 8 TeV searches	7,8	-	binary

the signal strength modifier and σ and $\sigma^{\mathrm{SUSY}}(\theta)$ are the observed and predicted cross sections, respectively, while the third (*binary*) uses either of the first two kinds of result together with a signal significance measure Z, and is used for combining results from overlapping search regions. Table 2 lists the likelihood adopted for each analysis, while in the following, we describe the signal significance measure Z and the form of each of the three likelihoods.

Counts Likelihood For a single count analysis, the likelihood is given by

$$L(D^{\mathrm{CMS}}|\theta) = \int \mathrm{Poisson}(N|s(\theta)+b)\, p(b|B,\delta B)db, \tag{5}$$

where N is the observed count, $s(\theta)$ and b are the expected number of signal and background counts, respectively, and $B \pm \delta B$ is the estimated number of background event counts and its uncertainty. The prior density for b, $p(b|B,\delta B)$ is modeled as a gamma density, $\mathrm{gamma}(x;\alpha,\beta) = \beta \exp(-\beta x)(\beta x)^{\alpha-1}/\Gamma(\alpha)$, with α and β defined such that the mode and variance of the gamma density are B and δB^2, respectively. For analyses that yield multiple independent counts, the likelihood is the product of the likelihoods of the individual counts. For multi-count analyses, we neglect the correlations between the background predictions for the different search regions. Systematic effects on the signal counts are taken into account by varying the signal yield by multiplying it with a signal strength modifier μ with values $1-\delta\mu, 1, 1+\delta\mu$, where $\delta\mu$ is the percent value of the systematic uncertainty.

χ^2 Likelihood This likelihood is used for CMS searches that provide profile likelihoods, $T(\mu,\theta) \equiv L(D^{\mathrm{CMS}}|\mu,\theta,\hat{\nu}(\mu,\theta))$, for the signal strength modifier μ, where ν represents the nuisance parameters and $\hat{\nu}(\mu,\theta)$ their conditional maximum likelihood estimates, while $\hat{\mu}$ denotes the signal strength modifier that maximizes $T(\mu,\theta)$. According to Wilks' theorem [58], in the

asymptotic limit, the quantity $t = -2\ln[T(1,\theta)/T(\hat{\mu},\theta)]$ follows a χ^2 density with one degree of freedom,

$$L(D^{\text{CMS}}|\theta) \quad = \quad \exp(-t/2)/\sqrt{2\pi t}, \tag{6}$$

which we adopt as the CMS likelihood in this case. Signal systematics can again be incorporated by varying the value of μ.

Z-Significance This study uses a signal significance measure defined by

$$Z(\theta) = \text{sign}[\ln B_{10}(D,\theta)]\sqrt{2|\ln B_{10}(D,\theta)|}, \tag{7}$$

where

$$B_{10}(D,\theta) = \frac{L(D|\theta,H_1)}{L(D|H_0)} \tag{8}$$

is the local Bayes factor for data D, at point θ, and $L(D|\theta,H_1)$ and $L(D|H_0)$ are the likelihoods for the signal plus background (H_1) and background only (H_0) hypotheses, respectively. This measure is a signed Bayesian analog of the frequentist "n-sigma". In conventional language, the case $Z \gg 0$ would indicate the presence of a signal at "Z-sigma significance", while the case $Z \ll 0$ would indicate the absence of signal, i.e., an *exclusion*, at "Z-sigma significance". The Z-significance is the basis of the binary likelihood.

Binary Likelihood This likelihood is used for combining results from search regions in which data may not be mutually independent, for example, multiple counts from overlapping search regions. We first divide the data into subsets for which either a count or χ^2 likelihood can be calculated. For each subset l, with data D_l, we compute $Z_l(\theta)$ using Eq. (7). An overall significance measure, that includes all subsets under consideration, is defined by

$$Z(\theta) = Z_l(\theta), \text{ with } l \equiv \arg\max_j(|Z_j(\theta)|), \tag{9}$$

which is used to define the binary likelihood as follows,

$$L(D^{\text{CMS}}|\theta) = \begin{cases} 1 & \text{if } Z(\theta) > -1.64, \\ 0 & \text{if } Z(\theta) \leq -1.64. \end{cases} \tag{10}$$

Here, systematic uncertainties are incorporated by computing each $Z_j(\theta)$ by varying the value of μ, and using these recalculated $Z_j(\theta)$ to compute the binary likelihood. Although use of the binary likelihood entails a loss of information, it is a convenient approach in cases of non-disjoint data, where a proper likelihood calculation is not feasible without more information. In this study, we use binary likelihoods for monojet searches, which has overlapping search regions, and for combining the 7 TeV, 8 TeV and 7+8 TeV results, where the considered analyses use non-disjoint data.

In order to compute likelihoods and Z-significances, we need the expected signal counts for the search regions of every analysis under consideration, and for each of the 7200 pMSSM points. These counts are obtained by analyzing event samples generated using `PYTHIA6.4` [59] and processed with the CMS fast detector simulation program [60]. For each pMSSM point, 10000 events are simulated.

3.3 Presentation of results

In the next section, we present the results of our study using three different approaches for assessing what we have learned about the pMSSM. In the first approach, we compare the distributions of the Z-significances. In the second approach, we compare the prior and posterior densities of the pMSSM parameters. In the third approach, we use a measure of the parameter space that remains after inclusion of the CMS search results. This measure, the survival probability in a region Θ of the pMSSM parameter space, is defined by

$$\frac{\int_\Theta p(\theta) H(Z + 1.64) d\theta}{\int_\Theta p(\theta)\, d\theta}, \tag{11}$$

where $p(\theta)$ is either the prior or posterior density, H is the Heaviside step function with a threshold value $Z = -1.64$, which is motivated by the frequentist threshold for exclusion at the 95% confidence level.

4 Results

We start by presenting distributions of Z-significance in Fig. 1 for all the CMS searches included in this study: 8 TeV searches, combinations of 8 TeV searches, combinations of 7 TeV searches, and combinations of 7+8 TeV searches. The further a Z distribution is from zero, the greater the impact of the analysis on the pMSSM parameter space. As noted in Section 3, negative and positive values indicate a preference for the background only (H_0) and the signal plus background (H_1) hypotheses, respectively.

All 8 TeV searches lead to distributions with negative tails, indicating that each disfavors some region of the parameter space. The searches making the greatest impact are the HT+MHT and MT2 searches, which disfavor a significant portion of the parameter space. The MT2, HT+MET+b-jets, electroweak (EW) and opposite sign (OS) di-lepton searches, which yield modest excesses over the SM predictions, have Z-significances up to 3, and even 4, indicating the data are more consistent with small regions of the pMSSM space than with the SM.

As expected, the combined 8 TeV result has a greater impact than any individual analysis. Overall, the impact of the 7 TeV combined result is very small as indicated both by the high peak around zero, and from the very small difference between the 7 TeV and 7+8 TeV combined distributions. The dip around zero in the combined 8 TeV distribution arises from the way we combine Z-significances. As expressed in Eq. (9), the maximum Z-significance values are used in the combination.

Fig. 2 shows the impact of the CMS searches on our knowledge of the gluino mass. Plots (a)-(d) show marginalized distributions of the gluino mass. Posterior distributions obtained using three signal strength modifier values $\mu = 0.5, 1, 1.5$ illustrate the effect of a $\pm 50\%$ systematic uncertainty in the predicted SUSY cross sections. Plot (a) shows the strong impact of the inclusive analyses on the gluino mass distribution. The HT+MHT search strongly disfavors the region below 1200 GeV, while the MT2 search leads to a distribution with two preferred regions, one at relatively low mass, around 600 to 1000 GeV, and one above 1200 GeV. In plot (b) we observe that the other hadronic analyses also disfavor the low mass region, though to a lesser degree, while the leptonic analyses have no or very little impact on the gluino mass distribution. Plot (d) compares the prior distribution to posterior distributions after inclusion of the combined 7 TeV and combined 7+8 TeV data. The 7 TeV data already strongly disfavor the low mass region, a conclusion that is strengthened after adding the 8 TeV data. The enhancement induced

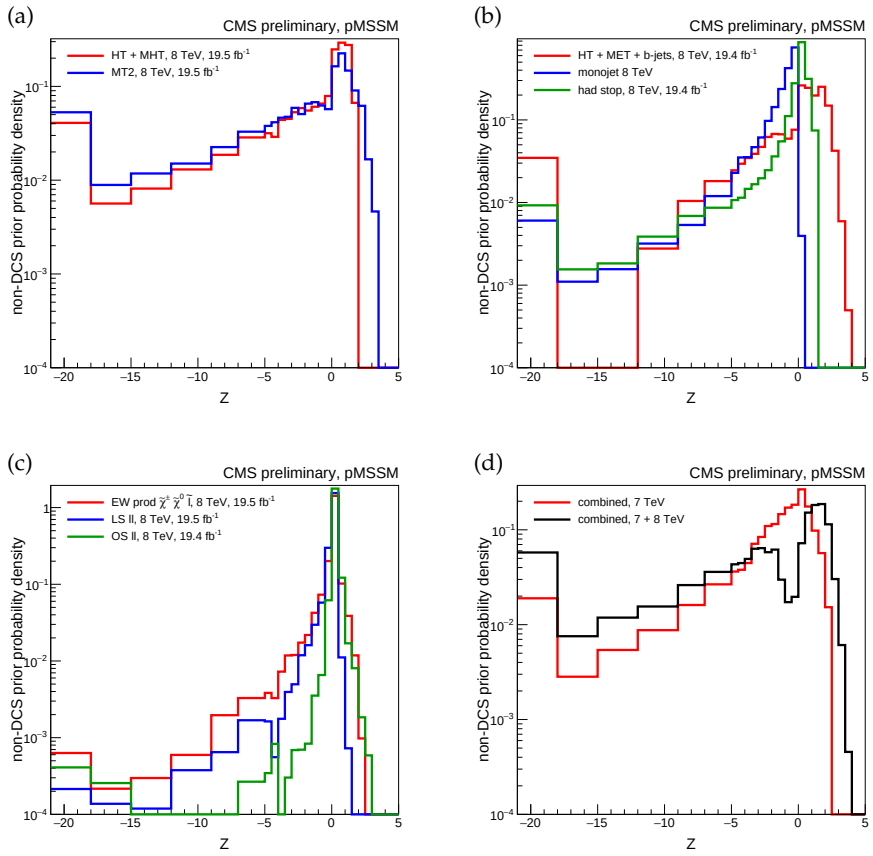

Figure 1: Z-significance distributions for the individual 8 TeV searches (a-c), and for 7 TeV combined and 7+8 TeV combined searches (d). The left-most bin contains the underflow entries.

by the MT2 search around the 600 to 1000 GeV region disappears in the combination since the other analyses do not show excesses of events and have higher sensitivity in this region.

Plot (e) in Fig. 2 shows the survival probability as a function of gluino mass for the combined 7 TeV, 8 TeV, and 7+8 TeV results. The survival probability reduces most notably when adding the combined 8 TeV results with the 7 TeV results; the contribution of the latter to the overall combination is almost negligible as can be seen by comparing the 8 TeV versus 7+8 TeV curves. CMS searches exclude all the pMSSM points we have considered with a gluino mass below 500 GeV, and can probe scenarios up to the highest masses covered in the scan. Of course, masses of order 3 TeV are not probed directly but rather through the production of lighter particles in the model. Including measurements of the Higgs boson signal strength and branching fractions in the prior leads to a moderate preference for scenarios with a negative value for the higgsino mass parameter μ. Finally, plot (f) shows the Z-significance versus gluino mass. There is a very slight negative correlation for positive Z values and gluino masses below 1.2 TeV — Z declines slightly as mass increases, which indicates that the small observed excess of events by the various searches are consistent with models with light gluinos.

Figs. 3 and 4 similarly summarize the impact of searches on the first and second generation left squark mass and the mass of the Lightest Colored SUSY Particle (LCSP), respectively. The picture is similar to that for the gluino mass. For both $\tilde{u}_L$ and the LCSP, the MT2 search shows a preference for masses from 500 to 1100 GeV. The overall impact of the searches on $\tilde{u}_L$ is less than the impact on the gluino mass owing to the more diverse gluino decay structure

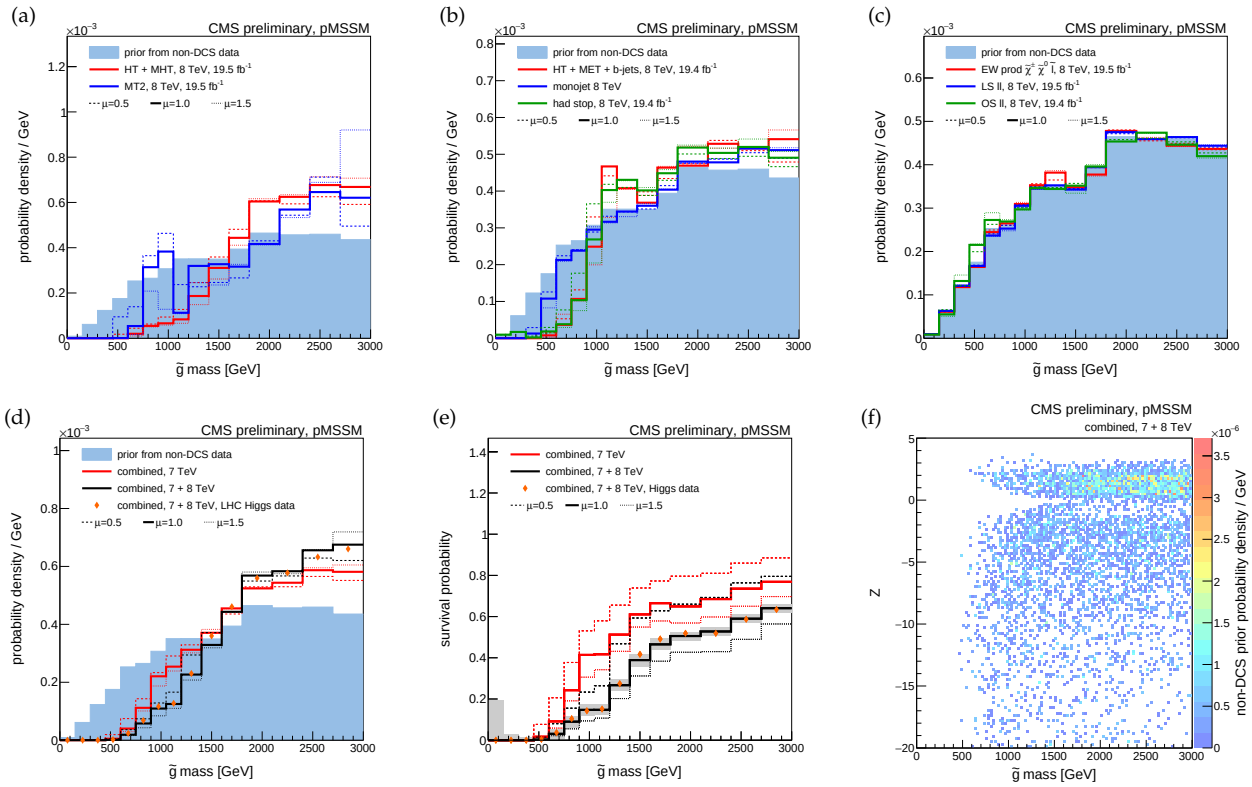

Figure 2: A summary of the impact of CMS searches on our knowledge of the gluino mass in the pMSSM parameter space. Plots (a)-(d) compare the non-DCS prior distribution of the gluino mass (blue filled histograms) to posterior distributions after data from various CMS searches (line histograms), where (d) shows the combined effect of CMS searches and the Higgs boson results. Plot (e) shows survival probabilities as a function of the gluino mass for various combinations of CMS data and data from Higgs boson measurements. Plot (f) shows the distribution of the gluino mass versus the Z-significance calculated from the combination of all searches.

that can be accessed by a greater number of searches. For the LCSP, the overall impact is the least because it has the least variation in decay channels, however, CMS searches can still conclusively exclude cases with LCSPs below 300 GeV. We also see that the searches can be sensitive to scenarios with LCSP masses up to ∼1.5 TeV. We find, again, that the Higgs boson results make a negligible contribution. As it is true of the gluino mass, there is a negative correlation between the Z-significances and the $\tilde{u}_L$ or LCSP masses for positive Z values and masses below 1200 GeV, but the correlation is stronger.

Fig. 5 illustrates what has been learned about the mass of the lightest top squark $\tilde{t}_1$. The difference between the prior and posterior distributions is minor. The reason is that the measurements of the $b \to s\gamma$ branching ratio (see Table 1) impose much stronger constraints on the mass of the $\tilde{t}_1$ than the LHC data do. This highlights the importance of using a prior that encodes as much experimental information as possible in order to arrive at a meaningful assessment of the added value of data from the LHC. The exception to the statement about the $\tilde{t}_1$ is the posterior distribution for the MT2 search which, relative to the non-DCS distribution, has a preference for low $\tilde{t}_1$ masses. In the distribution of the top squark mass versus Z, the positive Z values have a very slight negative correlation with the $\tilde{t}_1$ mass below 1200 GeV. The overall conclusion is that light stops with masses of the order of 500 GeV cannot be excluded.

Turning now to the electroweak sector, we first show, in Fig. 6, the effect of the CMS data on

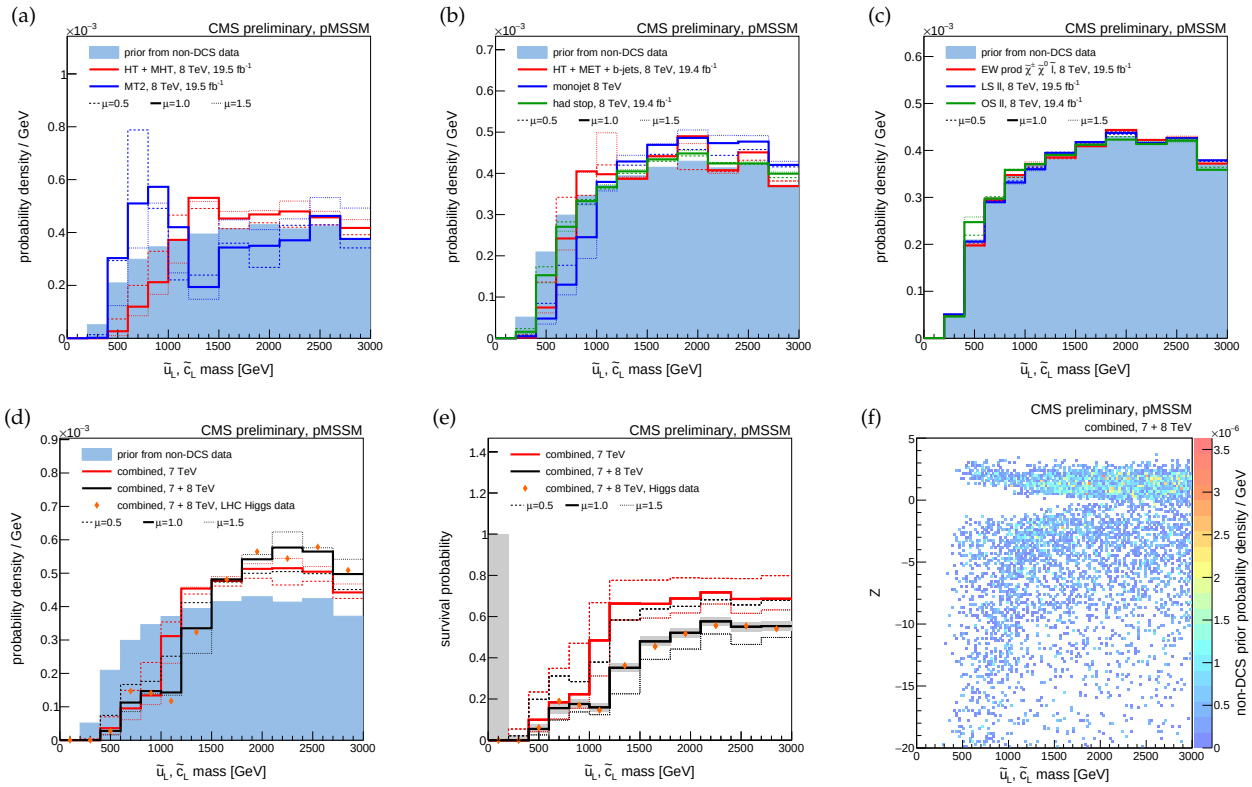

Figure 3: A summary of the impact of CMS searches on our knowledge of the $\tilde{u}_L$ quark mass in the pMSSM parameter space. Plots (a)-(d) compare the non-DCS prior distribution of the $\tilde{u}_L$ quark mass to posterior distributions after data from various CMS searches, where (d) shows the combined effect of CMS searches and the Higgs boson results. Plot (e) shows survival probabilities as a function of the $\tilde{u}_L$ quark mass for various combinations of CMS data and data from Higgs boson measurements. Plot (f) shows the distribution of the $\tilde{u}_L$ quark mass versus the Z-significance calculated from the combination of all searches. See Fig. 2 for a description of the shading.

our knowledge of the mass of the lightest neutralino $\tilde{\chi}_1^0$. We see that the hadronic inclusive searches strongly disfavor low $\tilde{\chi}_1^0$ masses; the hadronic searches targeting specific topologies also have an effect, although smaller, and the leptonic searches have a marginal impact. The 7+8 TeV combined distribution is very similar to the MT2 distribution, especially in the lower mass region, making this the most decisive search affecting our knowledge of the $\tilde{\chi}_1^0$ mass. The significant impact on the $\tilde{\chi}_1^0$ mass is indirect. Since $\tilde{\chi}_1^0$ is the lightest SUSY particle, its mass is constrained by the masses of the heavier sparticles. As CMS searches push the probability distributions for the colored particles to higher values, more phase space opens for $\tilde{\chi}_1^0$ and the $\tilde{\chi}_1^0$ distributions shift to higher values. The survival probability distribution shows that no $\tilde{\chi}_1^0$ mass is totally excluded by CMS. In general, the non-excluded points with light $\tilde{\chi}_1^0$ are those with heavy colored sparticles. The fact that the survival probability increases until a $\tilde{\chi}_1^0$ mass of $\sim$700 GeV shows that CMS searches are sensitive up to this mass value. The Higgs boson data disfavor neutralino masses below about 60 GeV, that is, the mass range in which invisible decays $h^0 \to \tilde{\chi}_1^0\tilde{\chi}_1^0$ could occur; this is visible in the first bin in plot (d) of Fig. 6 (See Ref. [36] for the current combined limits on the Higgs boson$\to$ invisible rate).

In the MSSM, the lightest chargino is degenerate with the lightest neutralino when $|M_1| \geq$

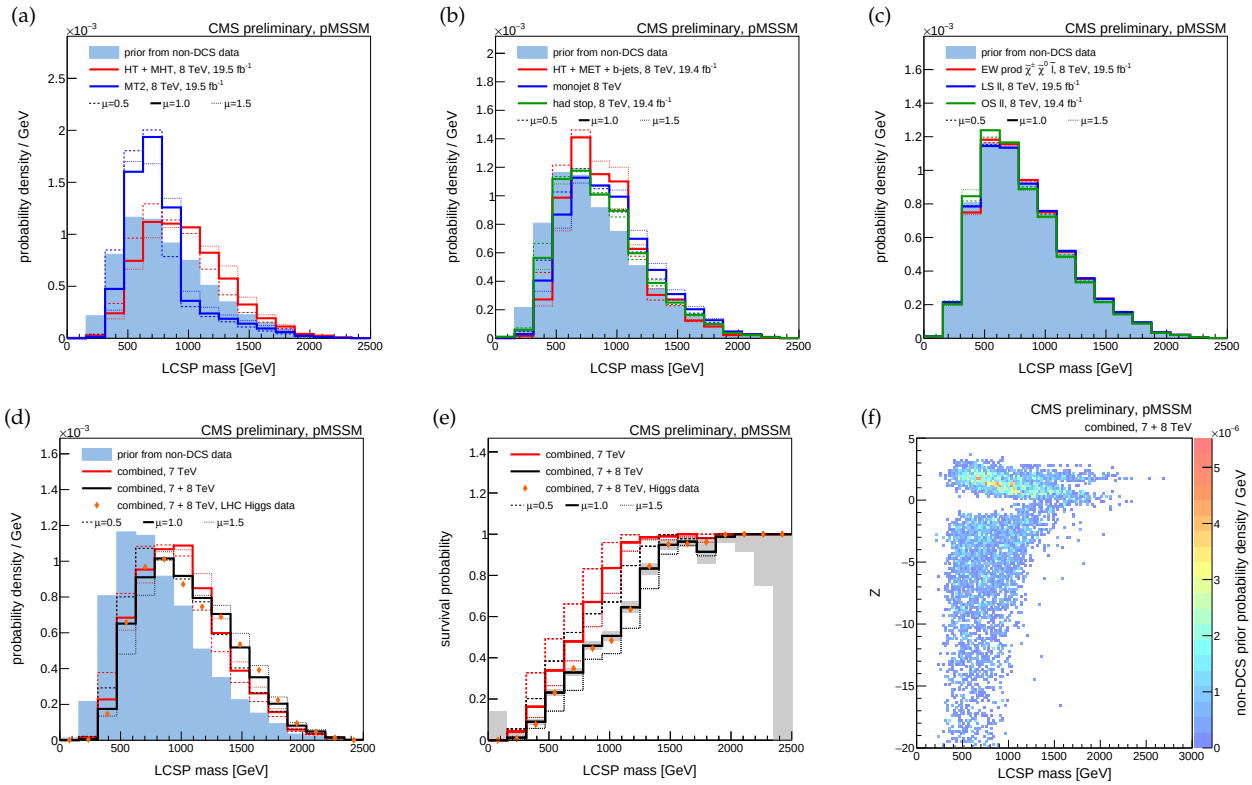

Figure 4: A summary of the impact of CMS searches on our knowledge of the mass of the Lightest Colored SUSY Particle (LCSP) in the pMSSM parameter space. Plots (a)-(d) compare the non-DCS prior distribution of the LCSP mass to posterior distributions after data from various CMS searches, where (d) shows the combined effect of CMS searches and the Higgs boson results. Plot (e) shows survival probabilities as a function of the LCSP mass for various combinations of CMS data and data from Higgs boson measurements. Plot (f) shows the distribution of the LCSP mass versus the Z-significance calculated from the combination of all searches. See Fig. 2 for a description of the shading.

$\min(|M_2|, |\mu|)$. Therefore, we define the Lightest Non Degenerate (LND) chargino as follows:

$$\text{LND } \chi^{\pm} = \begin{cases} \tilde{\chi}_1^{\pm} & \text{if } |M_1| < \min(|M_2|, |\mu|) \\ \tilde{\chi}_2^{\pm} & \text{if } |M_1| > \min(|M_2|, |\mu|) \end{cases}. \tag{12}$$

Fig. 7 summarizes what we have learned about the mass of the LND. Again, the impact of the CMS searches is found to be rather limited and no chargino mass can be reliably excluded. It is worth noticing the impact of the leptonic searches. In plot (c) of Fig. 7, the distributions differ from the non-DCS distribution, while these searches have negligible impact on most of the other SUSY observables and parameters considered in this study. We also note that the survival probability is lowest in the first bin where LND mass is between 0 and 200 GeV, but a small percentage of points still survive.

A more generic view is possible by looking at the overall CMS impact on the inclusive SUSY production cross section for 8 TeV, which is shown in Fig. 8. Before adding the CMS results, the most probable cross section is around 100 fb; the effect of the CMS SUSY searches is to reduce this value by an order of magnitude. The inclusive HT+MHT search has the largest individual contribution in this because of its ability to address a great diversity of final states comprising different sparticle compositions. The survival probability distribution confirms that CMS is

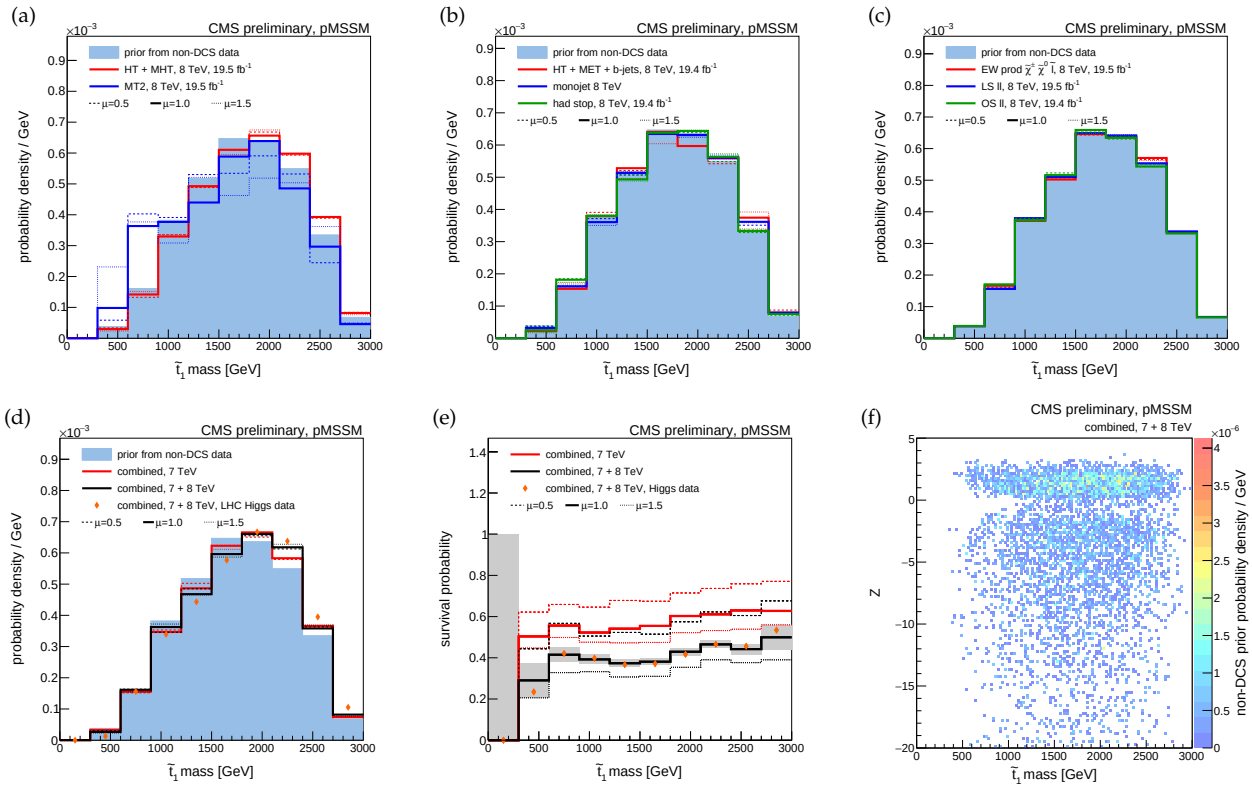

Figure 5: A summary of the impact of CMS searches on our knowledge of the $\tilde{t}_1$ quark mass in the pMSSM parameter space. Plots (a)-(d) compare the non-DCS prior distribution of the $\tilde{t}_1$ quark mass to posterior distributions after data from various CMS searches, where (d) shows the combined effect of CMS searches and the Higgs boson results. Plot (e) shows survival probabilities as a function of the $\tilde{t}_1$ quark mass for various combinations of CMS data and data from Higgs boson measurements. Plot (f) shows the distribution of the $\tilde{t}_1$ quark mass versus the Z-significance calculated from the combination of all searches. See Fig. 2 for a description of the shading.

sensitive to SUSY scenarios with total cross sections as low as 1 fb. The cross section is the variable found to correlate most strongly with the Z-significance, so we conclude that the cross section is the observable to which the analyses are most sensitive. The Z values above ~ 1 fb are all non-zero, which implies that CMS data are capable of making an impact above that value.

In Fig. 9, the non-DCS and post CMS distributions are compared after 7, 8 and 7+8 TeV data for several other important observables. We first note that the impact of the CMS data on the first and second generation right up squarks is lower than the corresponding left up squarks. This is because the left up squarks in the MSSM form doublets with mass-degenerate left down squarks, while the right up squarks and right down squarks are singlets and their masses are unrelated. Therefore, for the left up squarks, the CMS sensitivity for a given mass is increased by the left down squarks, which have the same mass. We also observe a mild impact on the bottom squark mass, where CMS disfavors masses below 400 GeV. The CMS searches also have some sensitivity to the selectron and stau masses, which comes from the leptonic searches. The impact on $\tilde{\chi}_2^0$ and $\tilde{\chi}_1^{\pm}$ masses is relatively larger, mostly due to the dedicated EW analyses. CMS SUSY searches have no impact on the light and heavy pseudoscalar Higgs boson masses. The impact of the Higgs data on the μ parameter comes primarily from the fact that the measured signal strength for $Vh \to b\bar{b}$ (where V is a W or a Z boson) is currently slightly below one.

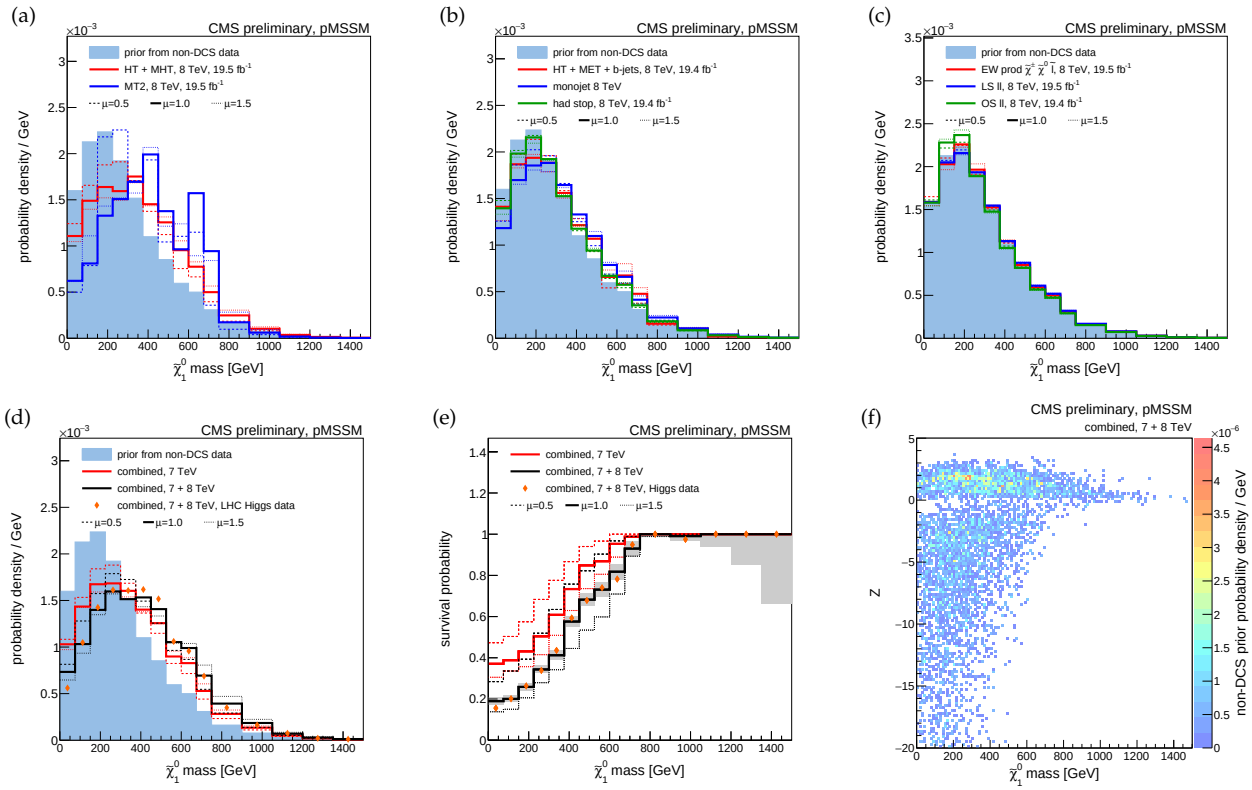

Figure 6: A summary of the impact of CMS searches on our knowledge of the $\widetilde{\chi}_1^0$ mass in the pMSSM parameter space. Plots (a)-(d) compare the non-DCS prior distribution of the $\widetilde{\chi}_1^0$ mass to posterior distributions after data from various CMS searches, where (d) shows the combined effect of CMS searches and the Higgs boson results. Plot (e) shows survival probabilities as a function of the $\widetilde{\chi}_1^0$ mass for various combinations of CMS data and data from Higgs boson measurements. Plot (f) shows the distribution of the $\widetilde{\chi}_1^0$ mass versus the Z-significance calculated from the combination of all searches. See Fig. 2 for a description of the shading.

In a SUSY model, this requires that radiative corrections reduce the bottom Yukawa coupling, thereby creating a preference for $\mu < 0$ [38]. The $\tan\beta$ distribution is largely unaffected by both the CMS SUSY searches and the current Higgs boson data evaluated via `Lilith1.01`.

We also investigate the effect of CMS searches on some dark matter-related observables. The bottom row of Fig. 10 shows distributions of the dark matter relic density, the spin-dependent direct detection cross section, and spin-independent direct detection cross section.

4.1 Correlations between pMSSM parameters

A virtue of high-dimensional models like the pMSSM is that they enable the examination of correlations between parameters not possible in the context of more constrained models.

Fig. 11 compares marginalized distributions in 2-dimensions of non-DCS (left) to post-CMS distributions (middle), and also shows the post-CMS to non-DCS survival probability (right) for several observable pairs. The first two rows show that the CMS impact on our knowledge of the $\widetilde{\chi}_1^0$ mass is strongly correlated with the gluino or the LCSP mass. Since $\widetilde{\chi}_1^0$ is the LSP, light colored particles imply a light $\widetilde{\chi}_1^0$. Consequently, since colored particles are more dominant in the pMSSM than in constrained models, the disfavoring of light colored sparticles implies the disfavoring of a light $\widetilde{\chi}_1^0$. In the last row, we see that the $\widetilde{\chi}_1^0$ mass is correlated most strongly with the cross section and that light $\widetilde{\chi}_1^0$ LSPs are indeed disfavored for the reason just given.

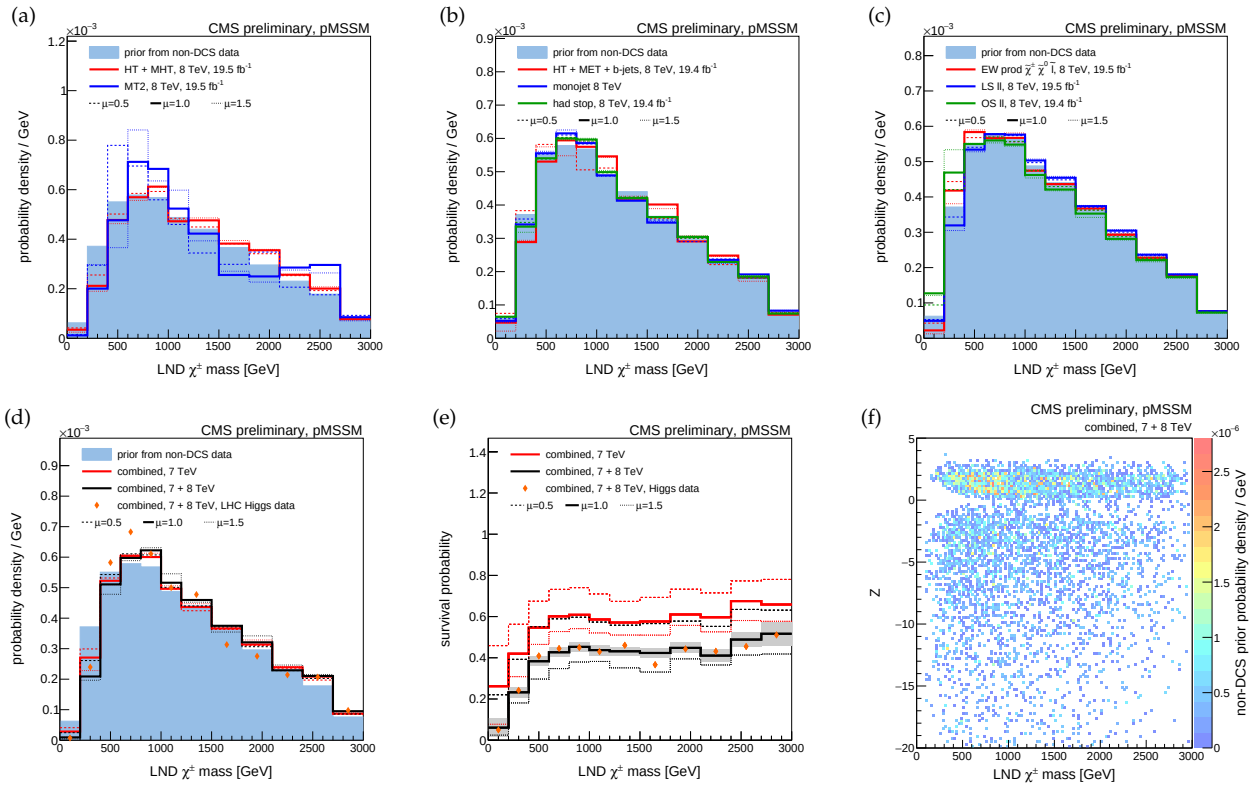

Figure 7: A summary of the impact of CMS searches on our knowledge of the the mass of the Lightest Non Degenerate (LND) chargino in the pMSSM parameter space. Plots (a)-(d) compare the non-DCS prior distribution of the LND $\widetilde{\chi}^{\pm}$ mass to posterior distributions after data from various CMS searches, where (d) shows the combined effect of CMS searches and the Higgs boson results. Plot (e) shows survival probabilities as a function of the LND $\widetilde{\chi}^{\pm}$ mass for various combinations of CMS data and data from Higgs boson measurements. Plot (f) shows the distribution of the LND $\widetilde{\chi}^{\pm}$ mass versus the Z-significance calculated from the combination of all searches. See Fig. 2 for a description of the shading.

We note, however, that scenarios with $\widetilde{\chi}^0_1$ masses around 100 GeV can still survive even though they have cross sections above 1 pb. In the third row, we show the probability distributions and survival probability for $\widetilde{\chi}^0_1$ versus $\tilde{t}_1$ mass. We see that, although the post-CMS probabilities shift towards higher values, the survival probabilities never really go down to zero. Although the current SMS scenarios exclude large parts of the $\tilde{t}_1$-$\widetilde{\chi}^0_1$ space for 100% $\tilde{t}_1$ branching ratios, we see that scenarios with light $\tilde{t}_1$ are still allowed in the full MSSM, as here the $\tilde{t}_1$ often has several decay modes available, which causes the individual branching ratios to be small. This closes the circle with the point made in the introduction about full versus SMS models.

5 Non-excluded regions in the pMSSM parameter space

Of the 7200 pMSSM points considered in this study, 3680 cannot be excluded by CMS analyses based on their Z-signficance, although more than half of these not-excluded points have a total cross section greater than 10 fb at $\sqrt{s}$ = 8 TeV. It is of interest to characterize this non-excluded subspace in order to shed light on why the CMS analyses are not sensitive to these points, and suggest ways to improve for future analyses in Run II. To this end, we decompose the non-excluded subspace into the dominant physical processes and follow with an idealized analysis of final state observables.

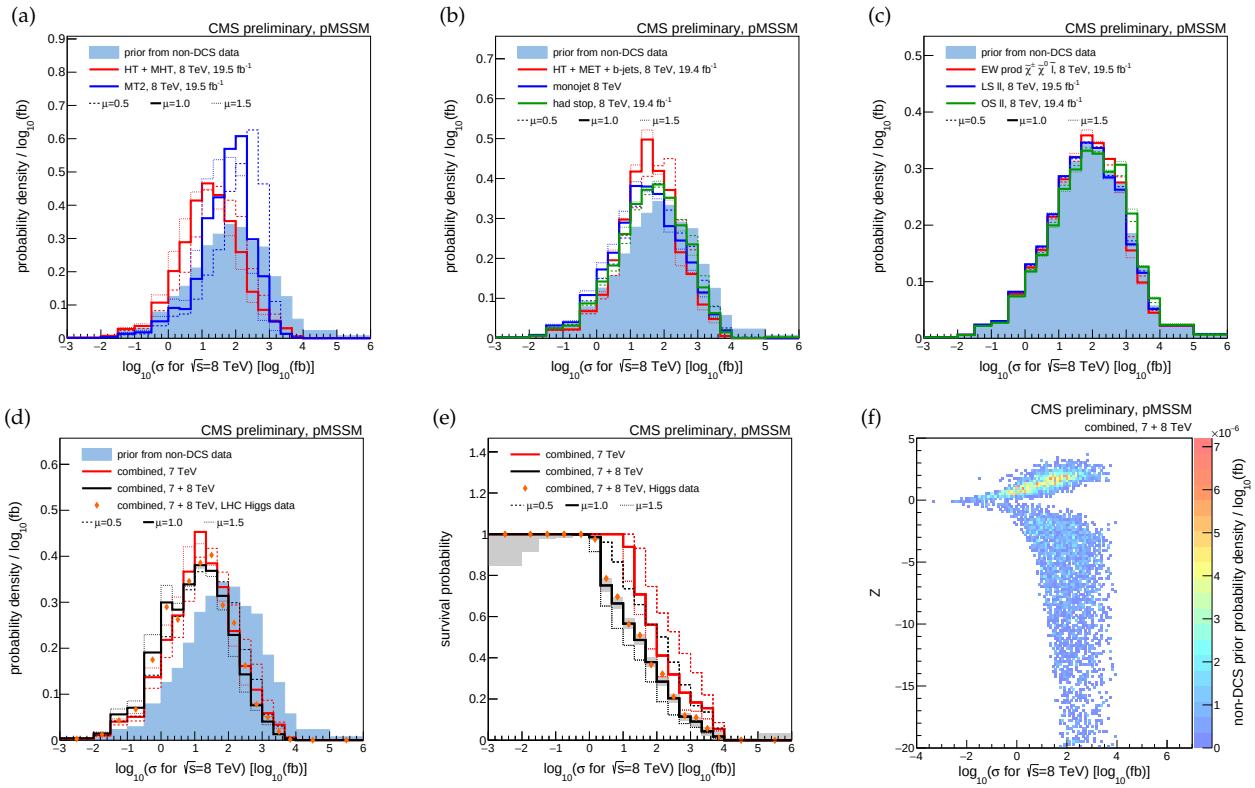

Figure 8: A summary of the impact of CMS searches on our knowledge of the the logarithm of inclusive cross section for inclusive sparticle production in 8 TeV pp collisions, $\log_{10}(\sigma for \sqrt{s} = 8\,\text{TeV})$, in the pMSSM parameter space. Plots (a)-(d) compare the non-DCS prior distribution of the $\log_{10}(\sigma for \sqrt{s} = 8\,\text{TeV})$ to posterior distributions after data from various CMS searches, where (d) shows the combined effect of CMS searches and the Higgs boson results. Plot (e) shows survival probabilities as a function of the $\log_{10}(\sigma for \sqrt{s} = 8\,\text{TeV})$ for various combinations of CMS data and data from Higgs boson measurements. Plot (f) shows the distribution of the $\log_{10}(\sigma for \sqrt{s} = 8\,\text{TeV})$ versus the Z-significance calculated from the combination of all searches. See Fig. 2 for a description of the shading.

For the decomposition, signal events are analyzed at the generator level for each model point, and the most frequent pair of SUSY particles produced directly from the proton-proton interaction is taken as the production mode for that model point. Then, the principal (dominant) topology for that point is built as a tree diagram starting from the pair of SUSY mother particles, and following the decay modes with the highest branching fractions until endpoints consisting of only standard model particles and LSPs are reached. Indices of particle charge, flavor, and handedness are ignored in the construction, with the exception of the third generation squarks/quarks, where flavor is considered. Over 100 distinct principal topologies are found among the total ∼7200 studied points, and the first twelve are listed in Fig. 12. Many of the principal topologies are seen to correspond to common SMS scenarios, while others depict more unusual scenarios with long decay chains.

The distribution of principal topologies for excluded and non-excluded points is given in Fig. 13a. It is seen that topologies involving direct gluino production (5 and 8) are excluded with a much higher frequency than they survive, and topologies with electroweak gaugino production (2, 3, and 10) survive with a higher frequency than they are excluded. Topologies with first generation squark production (1 and 7) survive and are excluded at a similar rate, and

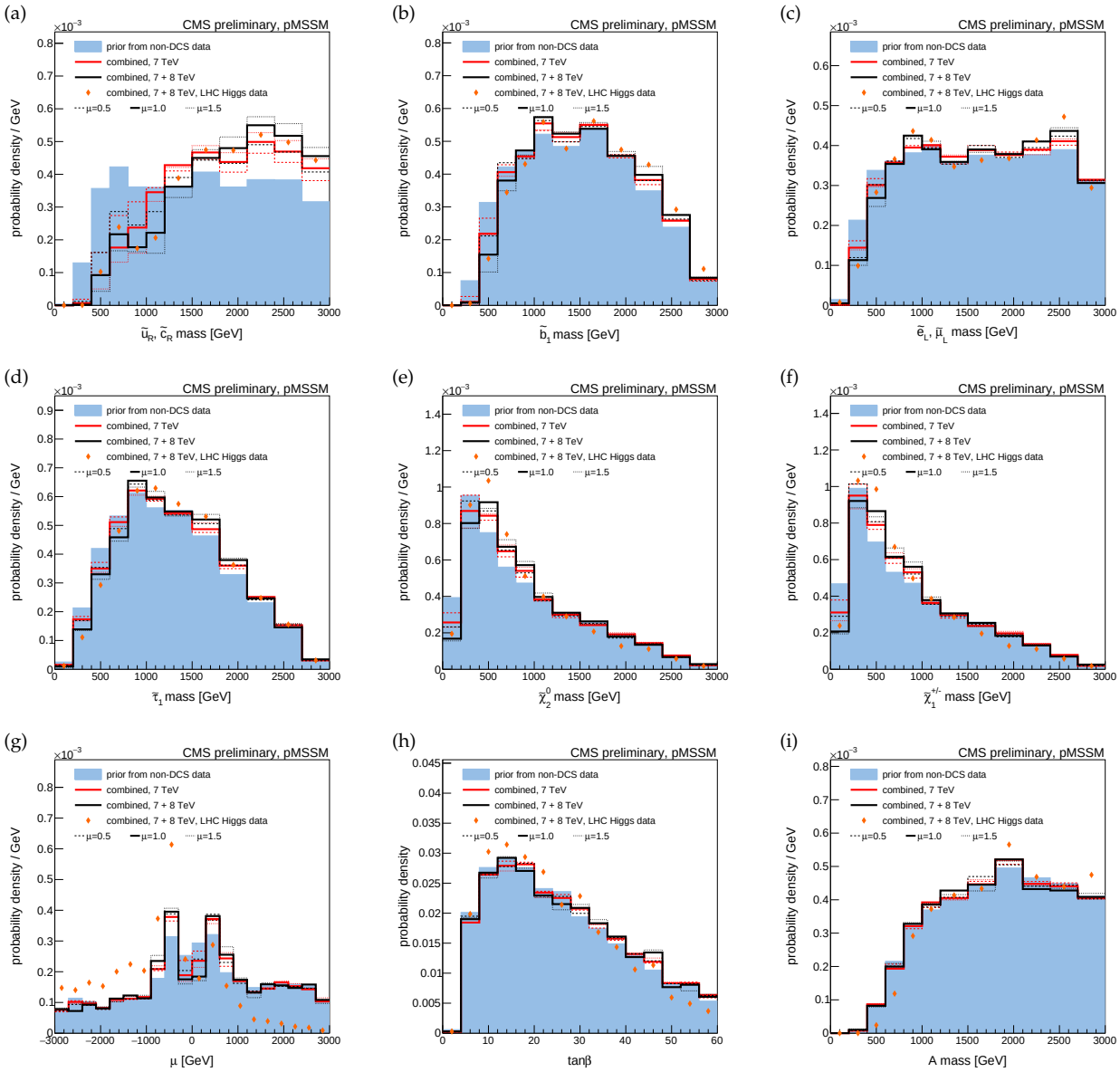

Figure 9: Comparison of prior and posterior distributions after several combinations of data from the CMS searches for the $\tilde{u}_R, \tilde{c}_R$ mass, $\tilde{b}1$ mass, $\tilde{e}_L, \tilde{\mu}_L$ mass, $\tilde{\tau}_1$ mass, $\widetilde{\chi}_2^0$ mass, $\widetilde{\chi}_1^{\pm}$ mass, μ parameter, $\tan\beta$, and A mass.

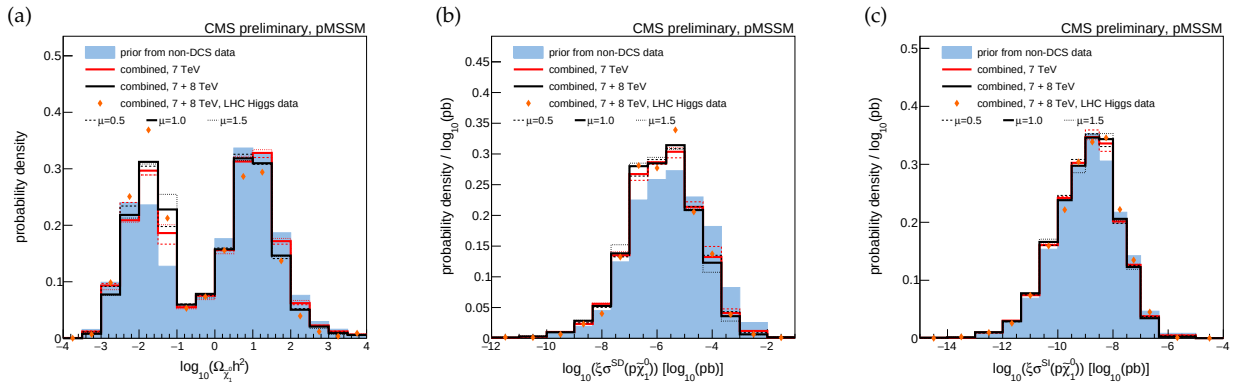

Figure 10: Comparison of prior and posterior distributions after several combinations of data from the CMS searches for $\Omega_{\tilde{\chi}_1^0}h^2$, $\xi\sigma^{SD}(p\tilde{\chi}_1^0)$, and $\xi\sigma^{SI}(p\tilde{\chi}_1^0)$.

topologies with slepton production (12) have exceptionally high survival rates. These trends are likely attributable to the difference in the production cross section between colored and non-colored particles for a given SUSY mass scale. The overflow bin, which contains a vast array of principal topologies, including modes of colored and non-colored particle production, indicates a survival rate approximately equal to the exclusion rate. The dominance, defined as the branching fraction to the principal topology, is given in Fig. 13b. Most values of the dominance are in the range of 0.05-0.6. The excluded and non-excluded values for the dominance are seen to agree to within the RMS of the distributions, indicating that the presence of a wide array of event signatures within a single model hypothesis does not significantly impact our ability to exclude such a model point.

Next, we characterize the non-excluded model space by the predicted final states in order to determine what signatures may become accessible at the LHC during Run II. In order to establish a well-defined set of final states, we define physics objects and event-level variables at the generator level. The final state objects and observables are defined as follows.

- Leptons: electrons, muons, or taus having a p_T greater than 5 GeV and an isolation less than 0.2. Here, isolation = $[(\Sigma_i p_{T_i}) - p_T]/\Sigma_i p_{T_i}$, where the sums run over all detector-visible particles i within an η-ϕ cone of 0.2 of the object ;
- Jets: particles clustered with the anti-kt jet algorithm [61] with distance parameter 0.5. The jets are required to have a p_T greater than 20 GeV;
- B-jets: jets matched within 0.5 to a B-hadron;
- MET: the missing transverse energy, calculated as the magnitude of the vector sum of the stable particles with p_T >5 GeV. Neutrinos and LSPs are not included in the sum.

We use a parallel coordinates visualization technique that enables the display of multiple dimensions. In Fig. 14, non-excluded points corresponding to the six most prevalent non-excluded principal topologies are shown. Axes are chosen to represent meaningful observables of the model points, and a number of distinct scenarios are seen to have survived the CMS analyses.

A minimum threshold of 20 fb has been applied to the 8 TeV signal cross sections in Fig. 14 to limit the scope to those points that could potentially still be probed with the Run I dataset using alternate or improved analysis strategies.

Points with principal topology 1, di-squark production, tend to have a large average MET, but moderate to low cross sections. Given the expectation that Run II will bring a general upward

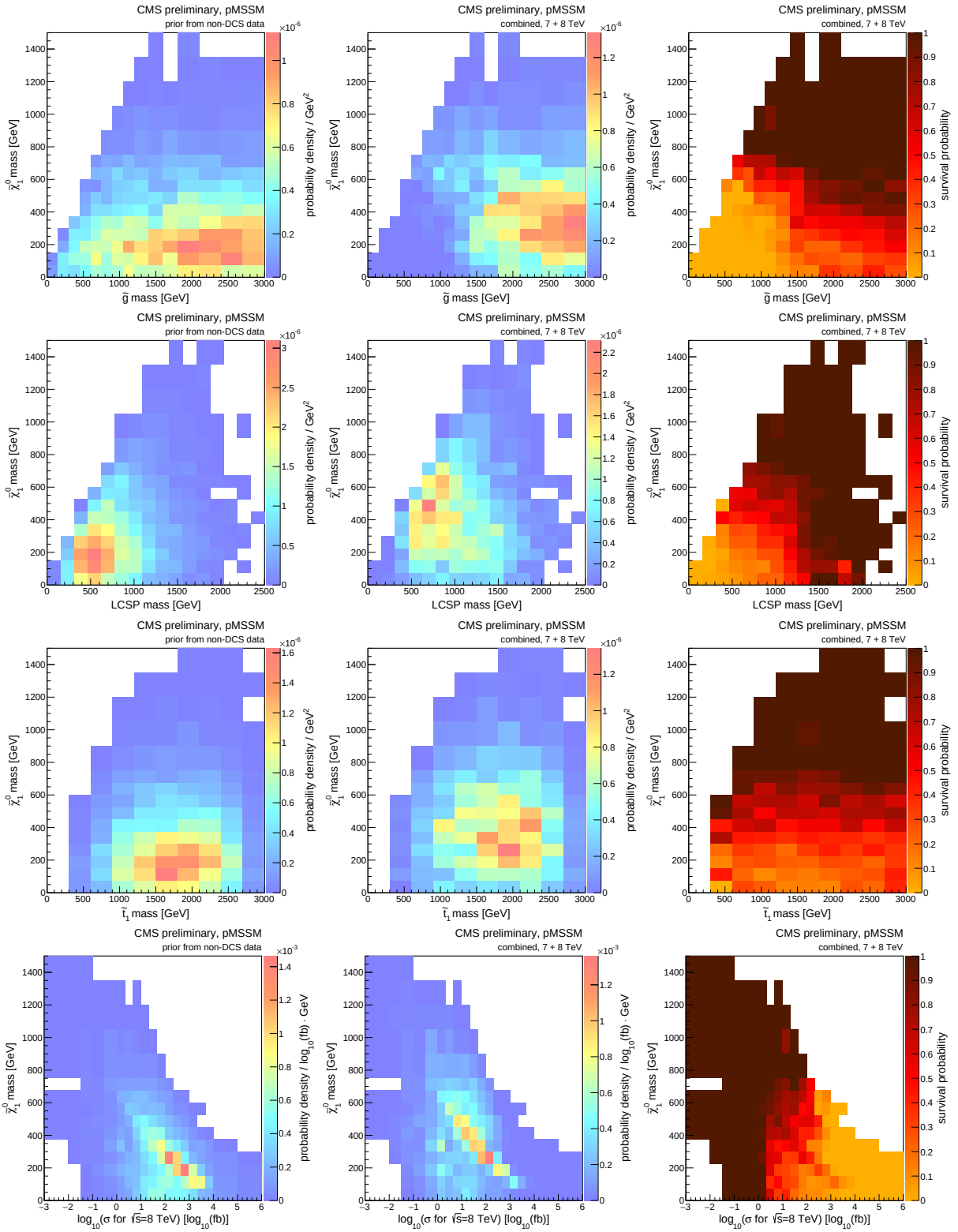

Figure 11: Marginalized non-DCS distributions (first column), compared with posterior distributions (second column) and survival probabilities (third column) after inclusion of all CMS data, are shown for the $\tilde{\chi}_1^0$ mass versus gluino mass (first row), versus the LCSP mass (second row), the stop (third row), and versus the logarithm of inclusive cross section for inclusive sparticle production at 8 TeV (bottom row).

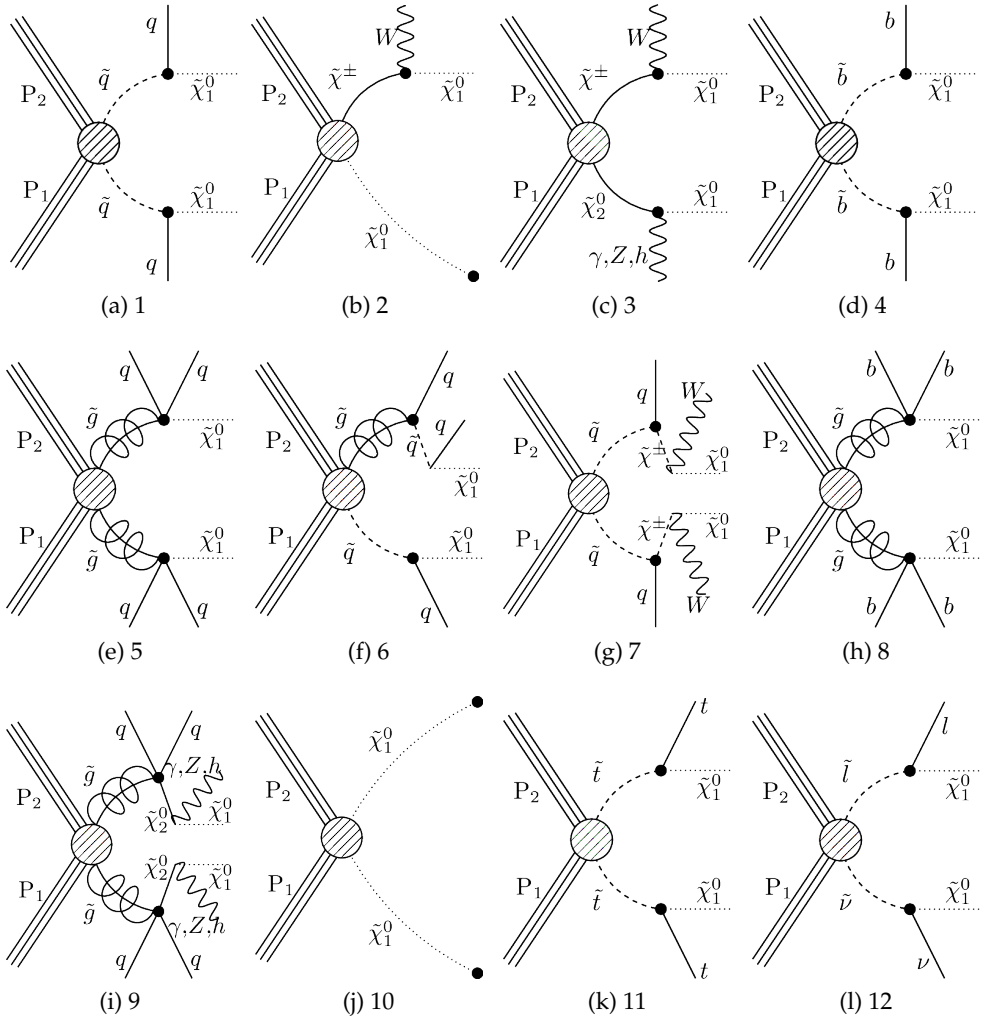

Figure 12: The twelve most common principal processes in the pMSSM, listed in order of their frequency in the set of all studied model points.

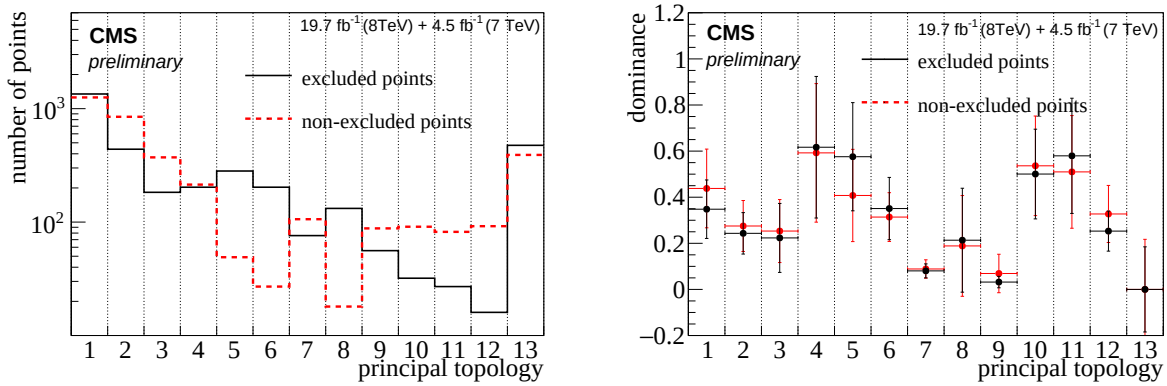

(a) (b)

Figure 13: The unweighted distribution of topologies for the excluded (black) and non-excluded (red) pMSSM points is given in (a). The dominance of the principal topologies is given in (b), where the value is the mean of the distribution of dominance values for all model points in the given bin, and the error bars are the RMS of this distribution.

shift in the cross sections, these high MET scenarios may soon become more accessible.

Points with principal topology 2, the asymmetric electroweak gaugino production mode, include scenarios with very large cross sections, but a limited number of physical observables; these points peak low in average multiplicity of jets, leptons, and in average MET.

Points with principal topology 3 and 10 tend to follow the trend profiled by topology 2, diverging primarily in the average leading lepton p_T and the lepton multiplicity. The close resemblance of topologies 10 and 2 could be attributable to the fact that the mass difference between the $\chi^{\pm}$ and the χ_1^0 can be very small, causing the ensuing off shell W boson to produce undetectably soft objects.

Points with principal topology 4, the production of two bottom squarks, are seen to have a moderate amount of MET with a large average number of b-jets, and relatively low cross sections.

Points with principal topologies 3 and 5, the most frequent modes involving gluinos, are associated with a large average number of jets, a moderate amount of MET, and relatively low cross sections. Once again, these signatures may rapidly become more accessible with the higher cross sections of Run II.

Points with principal topology 7 do not display distinct trends in the properties selected, which is due in part to these points having a low dominance value of around 0.1. Such model points have a diverse set of secondary topologies, which are not directly examined.

A general observation about the model points in Fig. 14 is the significant anti-correlation of observables, which manifests as the criss-crossing of lines between the axes. For example, model points with very high average MET tend to have very low cross sections, and vice versa. This is a consequence of the fact that, in the context of there being no significant observed excess of events in data, the surviving model points are those that do not exhibit a large number of physical observables, lest they would have been excluded.

With over 50% of all non-excluded points corresponding to cross sections of greater than 10 fb, it is critical to further examine the question, why were these points were not accessed in Run I? We attempt to answer by evaluating fiducial cross sections corresponding to a range of final

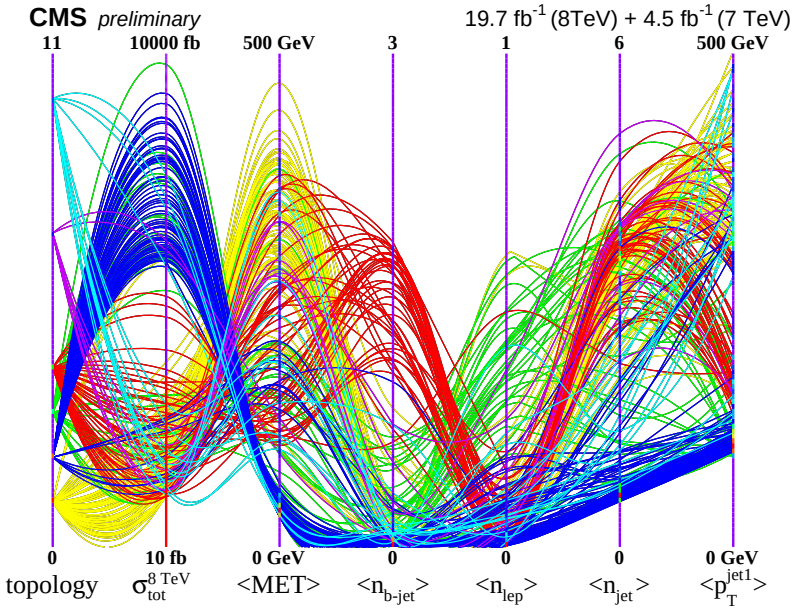

Figure 14: A parallel coordinates plot showing a few hundred selected non-excluded model points for the six most common principal topologies, with seven key properties. Properties are represented by vertical parallel axes, and a single model point corresponds to a curved line traversing the plot from left to right, intersecting each axis at the parameter value taken by the model point. From the left, the selected properties are: the principal topology, the 8 TeV signal production cross section (in $\log_{10}$ scale), the average value of the MET, the average number of b-jets, leptons, and jets, and finally, the average transverse momentum of the leading jet. Color is assigned based on the principal topology. Yellow codes for topology 1, blue for topology 2, green for 3, red for 4, violet for 7, and cyan for 10. Lines arching toward higher vertical positions typically indicate more "discoverable" scenarios.

state observables. The fiducial cross section σ_f^{SUSY} of a final state is defined as

$$\sigma_f^{SUSY} = \sigma_{tot}^{SUSY}(\theta) A(\theta). \tag{13}$$

where σ_{tot}^{SUSY} is the total signal production cross section at 8 TeV, and A is the acceptance times signal efficiency, that is, the fraction of simulated signal events passing a set of event-level criteria; both depend on the model point θ. We examine a set of final state observables that loosely correspond to trigger thresholds or signal regions of common SUSY searches.

Figures 15-17 show the impact of adjusting various thresholds on the fiducial cross sections of non-excluded points.

Different topologies manifest in large fiducial cross sections for different final states. For example, points with mostly first generation squark production give rise to large fiducial cross sections with high HT; and points with mostly electroweak gaugino production give rise to substantial fiducial cross sections with high MET, along with leptons.

Somewhat striking is the behavior of the MET fiducial cross section (Fig. 15), which can increase rapidly (by up to a factor of ten) as the threshold is relaxed from 200 to 100 GeV. It is apparent that many of the non-excluded regions are not accessible with thresholds of 200 GeV —a threshold that is commonly applied offline to achieve full efficiency with the triggers. The fiducial cross section decreases noticeably as the threshold is increased from 200 to 300 GeV.

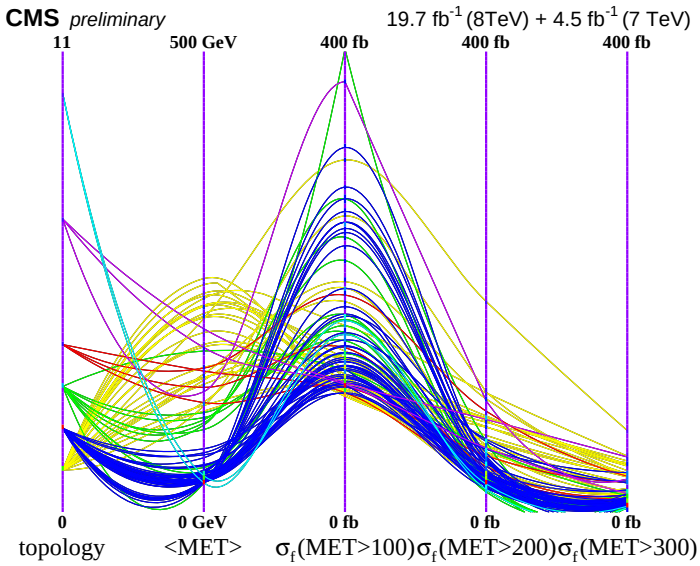

Figure 15: A parallel coordinates plot of the non-excluded pMSSM points with the axes set as the principal topology, the average MET, and the fiducial cross section (in linear scale) for various thresholds on the MET. All non-excluded points corresponding to topologies 1, 2, 3, 4, 7, and 10 that have a loose fiducial cross section greater than 100 fb are shown. Color is assigned to values of the principal topology in the same manner as in Fig. 14. Energy units are in GeV.

This serves as a caution against raising the the MET threshold above 200 GeV, as some key signatures are suppressed in doing so.

Similar behavior is seen for the HT fiducial cross section (Fig. 16). Quite large fiducial cross sections are seen for events having these final states when a threshold of 300 GeV is applied, but fall off substantially for higher thresholds. A thorough examination of the backgrounds would be necessary to select optimal values of the thresholds for targeting these points, and a lowering of the thresholds may only be possible if new techniques with better background rejection are developed.

6 Conclusions

We have investigated the impact of a representative set of the 7+8 TeV CMS SUSY searches on a potentially accessible sub-space of the pMSSM, a 19-dimensional proxy for the R-parity conserving weak-scale MSSM, defined at the SUSY scale. The sub-space, which is sampled using an MCMC method and a prior that incorporates data from precision measurements and non-direct CMS searches, covers sparticle masses up to about 3 TeV. Because this study relies on a fast detector simulation that does not provide an accurate description of massive long-lived charged particles, we work within a subspace of the pMSSM where the chargino lifetime $c\tau(\tilde{\chi}_1^{\pm})$ is less than 10 mm. The analyses included in this study span a variety of final states, which permit a broad exploration of the pMSSM, and by association the MSSM. The analyses include hadronic searches (HT + MHT, HT + MET + b-jets, MT2, monojets, stop), opposite-sign and like-sign leptonic searches, and leptonic searches for electroweak production of sparticles. We studied the effect of individual searches as well as various combinations including the combination of all the 7+8 TeV results. Searches based on the MT2 observable prove to be the most decisive in probing the mass of $\tilde{\chi}_1^0$, while, owing to the diversity of final states and decay chains to which they are sensitive, the HT+MHT searches make the largest overall contribution

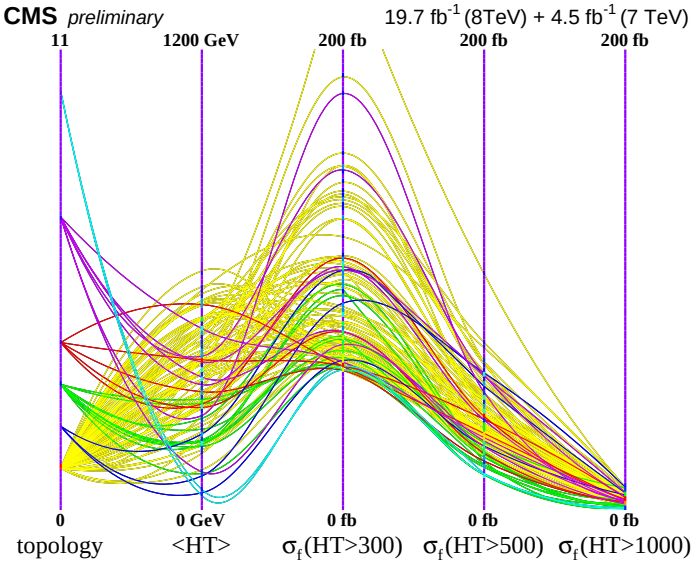

Figure 16: A parallel coordinates plot of the non-excluded pMSSM points with the axes set as the principal topology, the average HT, and the fiducial cross section (in linear scale) for various thresholds on the HT. All non-excluded points corresponding to topologies 1, 2, 3, 4, 7, and 10 that have a loose fiducial cross section greater than 60 fb are shown. Color is assigned to values of the principal topology in the same manner as in Fig. 14. Energy units are in GeV.

to our current state of knowledge of SUSY. We note that these statements are based on the observed impact of the searches in data, and not on their expected impact.

The CMS searches exclude all pMSSM points with a gluino mass less than 500 GeV and probe pMSSM points with gluino masses up to the highest masses covered in this scan using production processes involving the other lighter states. All pMSSM points are excluded in which the lightest colored supersymmetric particle has a mass less than 300 GeV, but the CMS searches remain sensitive up to masses as high as $\sim$1.5 TeV. Little has been learned about the mass of the lighter top squark, $\tilde{t}_1$, in spite of the fact that the stop-targeted searches considered exclude $\tilde{t}_1$ up to approximately 500 GeV in an SMS context. Constraints from previous experiments suppress the probability density in the light top squark regime at the level of the prior, and so a limited impact is observed on $m_{\tilde{t}_1}$. However, it is noted that the dedicated stop searches have an important impact on the other parameters. Searches targeting direct sbottom and stau production are not included in this interpretation, and we note that the inclusion of these searches would further constrain the pMSSM.

An interesting observation holds for the masses of the gluino, first and second generation squarks, charginos, and neutralinos; namely, that when the full diversity of SUSY spectra and decay chains are included, some of the existing limits purportedly placed on the masses of the SUSY particles are evaded. We should, therefore, exercise caution when drawing conclusions about what has been excluded using models based on simplified spectra, models that impose specific relationships between sparticle properties, or models that assume 100% branching ratios. The measurements of the Higgs boson mass and signal strengths do not alter the conclusions based on the CMS SUSY searches.

We investigated the non-excluded parameter space and found that half of the surviving model points have cross sections greater than 10fb. These points evade the analyses primarily because they are characterized by HT and MET that fall below the thresholds used in these analyses. The final states of non-excluded points have a significant contribution from Standard Model

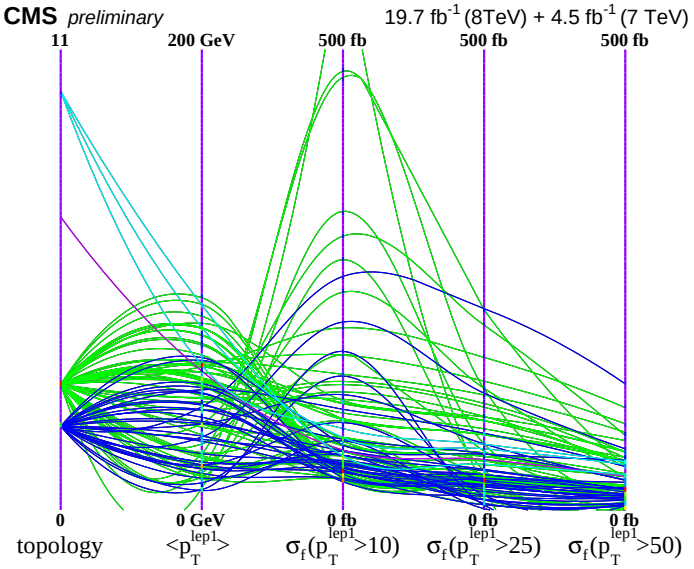

Figure 17: A parallel coordinates plot of the non-excluded pMSSM points with the axes set as the principal topology, the average leading lepton p_T, and the fiducial cross section (in linear scale) for various thresholds on the leading lepton p_T. All non-excluded points corresponding to topologies 1, 2, 3, 4, 7, and 10 that have a loose fiducial cross section greater than 30 fb are shown. Color is assigned to values of the principal topology in the same manner as in Fig. 14. Energy units are in GeV.

backgrounds, which presents a challenge for future analyses. Analyses that consider soft objects, small MET and HT, or new techniques to suppress or more precisely estimate background distributions, could have the potential to make an impact on the non-excluded points.

The above conclusions are robust statements about what current data tell us and do not tell us about the MSSM and demonstrate that a great deal more work is needed either to confirm or refute the weak-scale SUSY hypothesis.

A Original measurements in the MCMC

As mentioned in Section 3, several of the measurements used for defining the non-DCS likelihood were updated during the course of this study. To translate the effect of these results to the non-DCS likelihood, we reweighted the points with $w_i = L_i^{new}/L_i^{MCMC}$ for each observable i, where L_i^{MCMC} and L_i^{new} is the one calculated with the original value used in MCMC sampling. For completeness, the original values of the quantities that were updated are listed in Table 3. There was no update for observables $i = 4$, 7, and 10, which were used in the MCMC with the values as given in Table 3.

References

[1] ATLAS Collaboration, "Observation of a new particle in the search for the Standard Model Higgs boson with the ATLAS detector at the LHC", *Phys.Lett.* **B716** (2012) 1–29, doi:10.1016/j.physletb.2012.08.020, arXiv:1207.7214.

[2] CMS Collaboration, "Observation of a new boson at a mass of 125 GeV with the CMS experiment at the LHC", *Phys.Lett.* **B716** (2012) 30–61, doi:10.1016/j.physletb.2012.08.021, arXiv:1207.7235.

Table 3: Original values for the non-DCS constraints used in the MCMC scan, which were later updated to the values in Table 1.

i	Observable $\mu_i(\theta)$	Constraint $D_i^{\text{non-DCS}}$	Likelihood function $L(D_i^{\text{non-DCS}}\|\mu_i(\theta))$
1	$BR(b \to s\gamma)$ [62, 63]	$(3.55 \pm 0.23^{\text{stat}} \pm 0.24^{\text{th}} \pm 0.09^{\text{sys}}) \times 10^{-4}$	Gaussian
2	$BR(B_s \to \mu\mu)$ [64]	observed CLs curve from [64]	$d(1-CLs)/d(BR(B_s \to \mu\mu))$
3	$R(B_u \to \tau\nu)$[28, 44]	1.63 ± 0.54	Gaussian
5	m_t [65]	$173.3 \pm 0.5^{\text{stat}} \pm 1.3^{\text{sys}}$ GeV	Gaussian
8	m_h	pre-LHC: $m_h^{low} = 112$	1 if $m_h \geq m_h^{low}$ 0 if $m_h < m_h^{low}$

[3] S. P. Martin, "A Supersymmetry Primer", arXiv:hep-ph/9709356.

[4] D. Chung et al., "The soft supersymmetry breaking Lagrangian: Theory and applications", *Phys.Rept.* **407** (2005) 1–203, doi:10.1016/j.physrep.2004.08.032, arXiv:hep-ph/0312378.

[5] A. H. Chamseddine, R. L. Arnowitt, and P. Nath, "Locally Supersymmetric Grand Unification", *Phys.Rev.Lett.* **49** (1982) 970, doi:10.1103/PhysRevLett.49.970.

[6] R. Barbieri, S. Ferrara, and C. A. Savoy, "Gauge Models with Spontaneously Broken Local Supersymmetry", *Phys.Lett.* **B119** (1982) 343, doi:10.1016/0370-2693(82)90685-2.

[7] L. E. Ibanez, "Locally Supersymmetric SU(5) Grand Unification", *Phys.Lett.* **B118** (1982) 73, doi:10.1016/0370-2693(82)90604-9.

[8] L. J. Hall, J. D. Lykken, and S. Weinberg, "Supergravity as the Messenger of Supersymmetry Breaking", *Phys.Rev.* **D27** (1983) 2359–2378, doi:10.1103/PhysRevD.27.2359.

[9] P. Nath, "Twenty years of SUGRA", arxiv preprint, 2003. arXiv:hep-ph/0307123.

[10] G. L. Kane, C. F. Kolda, L. Roszkowski, and J. D. Wells, "Study of constrained minimal supersymmetry", *Phys.Rev.* **D49** (1994) 6173–6210, doi:10.1103/PhysRevD.49.6173, arXiv:hep-ph/9312272.

[11] H. Baer et al., "Multichannel search for minimal supergravity at $p\bar{p}$ and e^+e^- colliders", *Phys.Rev.* **D51** (1995) 1046–1050, doi:10.1103/PhysRevD.51.1046, arXiv:hep-ph/9408265.

[12] J. Alwall, P. Schuster, and N. Toro, "Simplified Models for a First Characterization of New Physics at the LHC", *Phys.Rev.* **D79** (2009) 075020, doi:10.1103/PhysRevD.79.075020, arXiv:0810.3921.

[13] LHC New Physics Working Group, "Simplified Models for LHC New Physics Searches", *J.Phys.* **G39** (2012) 105005, doi:10.1088/0954-3899/39/10/105005, arXiv:1105.2838.

[14] CMS Collaboration, "Interpretation of Searches for Supersymmetry with simplified Models", *Phys.Rev.* **D88** (2013) 052017, doi:10.1103/PhysRevD.88.052017, arXiv:1301.2175.

[15] MSSM Working Group, "The Minimal supersymmetric standard model: Group summary report", arXiv:hep-ph/9901246.

[16] S. Sekmen et al., "Interpreting LHC SUSY searches in the phenomenological MSSM", *JHEP* **02** (2012) 075, doi:10.1007/JHEP02(2012)075, arXiv:1109.5119.

[17] CMS Collaboration, "Search for Supersymmetry at the LHC in Events with Jets and Missing Transverse Energy", *Phys.Rev.Lett.* **107** (2011) 221804, doi:10.1103/PhysRevLett.107.221804, arXiv:1109.2352.

[18] CMS Collaboration, "Search for new physics with same-sign isolated dilepton events with jets and missing transverse energy", *Phys.Rev.Lett.* **109** (2012) 071803, doi:10.1103/PhysRevLett.109.071803, arXiv:1205.6615.

[19] CMS Collaboration, "Search for new physics in events with opposite-sign leptons, jets, and missing transverse energy in pp collisions at $\sqrt{s} = 7$ TeV", *Phys.Lett.* **B718** (2013) 815–840, doi:10.1016/j.physletb.2012.11.036, arXiv:1206.3949.

[20] C. P. Robert, "The Bayesian Choice: from Decision-Theoretic Foundations to Computational Implementation". Springer Verlag, New York, 2nd ed. edition, 2007.

[21] A. O'Hagan, "Bayesian Inference". Number Vol. 2B in Kendall's Advanced Theory of Statistics. Edward Arnold, London, 1994.

[22] C. Das and M. Parida, "New formulas and predictions for running fermion masses at higher scales in SM, 2 HDM, and MSSM", *Eur.Phys.J.* **C20** (2001) 121–137, doi:10.1007/s100520100628, arXiv:hep-ph/0010004.

[23] A. A. Markov, "Extension of the limit theorems of probability theory to a sum of variables connected in a chain". reprinted in Appendix B of: R. Howard, *Dynamic Probabilistic Systems, volume 1: Markov Chains*, John Wiley and Sons, 1971.

[24] Metropolis, N. and Rosenbluth, A. W. and Rosenbluth, M. N. and Teller, A. H. and Teller, E., "Equation of State Calculations by Fast Computing Machines", *J. Chem. Phys* **21** (1953) 1087–1092, doi:{10.1063/1.1699114}.

[25] W. K. Hastings, "Monte Carlo sampling methods using Markov chains and their applications", *Biometrika* **57** (1970), no. 1, 97–109, doi:10.1093/biomet/57.1.97.

[26] B. A. Berg, "Markov chain monte carlo simulations and their statistical analysis". World Scientific, 2004.

[27] B. Allanach, "SOFTSUSY: a program for calculating supersymmetric spectra", *Comput.Phys.Commun.* **143** (2002) 305–331, doi:10.1016/S0010-4655(01)00460-X, arXiv:hep-ph/0104145.

[28] F. Mahmoudi, "SuperIso v2.3: A Program for calculating flavor physics observables in Supersymmetry", *Comput.Phys.Commun.* **180** (2009) 1579–1613, doi:10.1016/j.cpc.2009.02.017, arXiv:0808.3144.

[29] G. Belanger, F. Boudjema, A. Pukhov, and A. Semenov, "MicrOMEGAs: A Program for calculating the relic density in the MSSM", *Comput.Phys.Commun.* **149** (2002) 103–120, doi:10.1016/S0010-4655(02)00596-9, arXiv:hep-ph/0112278.

[30] G. Belanger, F. Boudjema, A. Pukhov, and A. Semenov, "micrOMEGAs: Version 1.3", *Comput.Phys.Commun.* **174** (2006) 577–604, doi:10.1016/j.cpc.2005.12.005, arXiv:hep-ph/0405253.

[31] G. Belanger, F. Boudjema, A. Pukhov, and A. Semenov, "Dark matter direct detection rate in a generic model with micrOMEGAs 2.2", *Comput.Phys.Commun.* **180** (2009) 747–767, doi:10.1016/j.cpc.2008.11.019, arXiv:0803.2360.

[32] M. Muhlleitner, A. Djouadi, and Y. Mambrini, "SDECAY: A Fortran code for the decays of the supersymmetric particles in the MSSM", *Comput.Phys.Commun.* **168** (2005) 46–70, doi:10.1016/j.cpc.2005.01.012, arXiv:hep-ph/0311167.

[33] A. Djouadi, J. Kalinowski, and M. Spira, "HDECAY: A Program for Higgs boson decays in the standard model and its supersymmetric extension", *Comput.Phys.Commun.* **108** (1998) 56–74, doi:10.1016/S0010-4655(97)00123-9, arXiv:hep-ph/9704448.

[34] ATLAS Collaboration, G. Aad et al., "Updated coupling measurements of the Higgs boson with the ATLAS detector using up to 25 fb1 of proton-proton collision data", 2014.

[35] CMS Collaboration, "Precise determination of the mass of the Higgs boson and tests of compatibility of its couplings with the standard model predictions using proton collisions at 7 and 8 TeV", *Eur.Phys.J.* **C75** (2015), no. 5, 212, doi:10.1140/epjc/s10052-015-3351-7, arXiv:1412.8662.

[36] J. Bernon, B. Dumont, and S. Kraml, "Status of Higgs couplings after run 1 of the LHC", *Phys.Rev.* **D90** (2014), no. 7, 071301, doi:10.1103/PhysRevD.90.071301, arXiv:1409.1588.

[37] J. Bernon and B. Dumont, "Lilith: a tool for constraining new physics from Higgs measurements", arXiv:1502.04138.

[38] B. Dumont, J. F. Gunion, and S. Kraml, "The phenomenological MSSM in view of the 125 GeV Higgs data", *Phys.Rev.* **D89** (2014) 055018, doi:10.1103/PhysRevD.89.055018, arXiv:1312.7027.

[39] P. Z. Skands et al., "SUSY Les Houches accord: Interfacing SUSY spectrum calculators, decay packages, and event generators", *JHEP* **0407** (2004) 036, doi:10.1088/1126-6708/2004/07/036, arXiv:hep-ph/0311123.

[40] HFAG2013. "http://www.slac.stanford.edu/xorg/hfag/rare/2013/radll/OUTPUT/TABLES/radll.pdf.

[41] LHCb, CMS Collaboration, "Observation of the rare $B^0_s \to \mu^+\mu^-$ decay from the combined analysis of CMS and LHCb data", *Nature* **522** (2015) 68–72, doi:10.1038/nature14474, arXiv:1411.4413.

[42] K. Hagiwara et al., "$(g-2)_\mu$ and $\alpha(M_Z^2)$ re-evaluated using new precise data", *J.Phys.* **G38** (2011) 085003, doi:10.1088/0954-3899/38/8/085003, arXiv:1105.3149.

[43] Tevatron Electroweak Working Group, CDF and D0 Collaborations, "Combination of CDF and DO results on the mass of the top quark using up to 8.7 fb^{-1} at the Tevatron", arXiv:1305.3929.

[44] Particle Data Group, "Review of particle physics", *J.Phys.* **G37** (2010) 075021, doi:10.1088/0954-3899/37/7A/075021.

[45] Joint LEP2 SUSY Working Group, the Aleph, Delphi, L3 and Opal Collaborations. http://lepsusy.web.cern.ch/lepsusy/.

[46] CMS Collaboration, "Search for new physics in the multijet and missing transverse momentum final state in proton-proton collisions at $\sqrt{s} = 7$ TeV", *Phys.Rev.Lett.* **109** (2012) 171803, doi:10.1103/PhysRevLett.109.171803, arXiv:1207.1898.

[47] CMS Collaboration, "Search for supersymmetry in events with b-quark jets and missing transverse energy in pp collisions at 7 TeV", *Phys.Rev.* **D86** (2012) 072010, doi:10.1103/PhysRevD.86.072010, arXiv:1208.4859.

[48] CMS Collaboration, "Search for electroweak production of charginos and neutralinos using leptonic final states in pp collisions at $\sqrt{s} = 7$ TeV", *JHEP* **11** (2012) 147, doi:10.1007/JHEP11(2012)147, arXiv:1209.6620.

[49] CMS Collaboration, "Search for new physics in the multijet and missing transverse momentum final state in proton-proton collisions at $\sqrt{s}$= 8 TeV", *JHEP* **06** (2014) 055, doi:10.1007/JHEP06(2014)055, arXiv:1402.4770.

[50] CMS Collaboration, "Search for supersymmetry in hadronic final states using MT2 in pp collisions at $\sqrt{s} = 7$ TeV", *JHEP* **1210** (2012) 018, doi:10.1007/JHEP10(2012)018, arXiv:1207.1798.

[51] CMS Collaboration, "Search for gluino mediated bottom- and top-squark production in multijet final states in pp collisions at 8 TeV", *Phys.Lett.* **B725** (2013) 243–270, doi:10.1016/j.physletb.2013.06.058, arXiv:1305.2390.

[52] CMS Collaboration, "Search for dark matter, extra dimensions, and unparticles in monojet events in protonproton collisions at $\sqrt{s} = 8$ TeV", *Eur.Phys.J.* **C75** (2015), no. 5, 235, doi:10.1140/epjc/s10052-015-3451-4, arXiv:1408.3583.

[53] CMS Collaboration, "Search for top squarks decaying to a charm quark and a neutralino in events with a jet and missing transverse momentum",.

[54] CMS Collaboration, "Search for top squarks in multijet events with large missing momentum in proton-proton collisions at 8 TeV",.

[55] CMS Collaboration, "Search for physics beyond the standard model in events with two leptons, jets, and missing transverse momentum in pp collisions at sqrt(s) = 8 TeV", *JHEP* **1504** (2015) 124, doi:10.1007/JHEP04(2015)124, arXiv:1502.06031.

[56] CMS Collaboration, "Search for new physics in events with same-sign dileptons and jets in pp collisions at $\sqrt{s}$ = 8 TeV", *JHEP* **01** (2014) 163, doi:10.1007/JHEP01(2015)014, 10.1007/JHEP01(2014)163, arXiv:1311.6736.

[57] CMS Collaboration, "Searches for electroweak production of charginos, neutralinos, and sleptons decaying to leptons and W, Z, and Higgs bosons in pp collisions at 8 TeV", *Eur.Phys.J.* **C74** (2014), no. 9, 3036, doi:10.1140/epjc/s10052-014-3036-7, arXiv:1405.7570.

[58] S. Wilks, "The Large-Sample Distribution of the Likelihood Ratio for Testing Composite Hypotheses", *Annals Math.Statist.* **9** (1938), no. 1, 60–62, doi:10.1214/aoms/1177732360.

[59] T. Sjostrand, S. Mrenna, and P. Z. Skands, "PYTHIA 6.4 Physics and Manual", *JHEP* **0605** (2006) 026, doi:10.1088/1126-6708/2006/05/026, arXiv:hep-ph/0603175.

[60] CMS Collaboration, "The fast simulation of the CMS detector at LHC", *J.Phys.Conf.Ser.* **331** (2011) 032049, doi:10.1088/1742-6596/331/3/032049.

[61] M. Cacciari, G. P. Salam, and G. Soyez, "The Anti-k(t) jet clustering algorithm", *JHEP* **0804** (2008) 063, doi:10.1088/1126-6708/2008/04/063, arXiv:0802.1189.

[62] Heavy Flavor Averaging Group, "Averages of B-Hadron, C-Hadron, and tau-lepton properties as of early 2012", arXiv:1207.1158.

[63] M. Misiak et al., "Estimate of B(anti-B $\to$ X(s) gamma) at O(alpha(s)^2)", *Phys.Rev.Lett.* **98** (2007) 022002, doi:10.1103/PhysRevLett.98.022002, arXiv:hep-ph/0609232.

[64] ATLAS, CMS and LHCb Collaborations, "Search for the rare decays Bs and B0 to dimuons at the LHC with the ATLAS, CMS and LHCb experiments", cms physics analysis summary, 2012.

[65] CMS Collaboration, "LHC Combination: Top mass", CMS Physics Analysis Summary CMS-PAS-TOP-12-001, 2012.